Int J Theor Phys (2010) 49: 1823–1862
DOI 10.1007/s10773-010-0363-9

Entangled Finite Dimensional Pair Coherent States and Their Applications

A.-S.F. Obada · E.M. Khalil

Received: 6 January 2010 / Accepted: 14 April 2010 / Published online: 4 May 2010

Abstract Intermediate states of electromagnetic field are reviewed. It is a type of the correlated two-mode states (converter state). Based on the resonant ion-cavity interaction, we propose a scheme to generate these states revealing their connection with the converter state. The practical feasibility of this method is also discussed. We discuss nonclassicality of a finite dimensional pair coherent states in terms of sub-Poissonian photon statistics as well as the negativity of the Wigner function after deriving the analytic expression for the Wigner function. We explore a superposition of two finite dimensional pair coherent states. We show that such states possess inherent nonclassical properties such as sub-Poissonian distribution, anti-correlation between the two modes and violation of Cauchy-Schwarz inequalities. The s-parameterized characteristic function (CF) is considered. The phase distribution in the framework of Pegg and Barnett formalism, W-function and Q-function are discussed. Furthermore, a two-level atom in interaction with a two-mode quantized electromagnetic fields besides a frequency converter interaction initially prepared in an entangled two-mode coherent state is presented. Exact solution of the wave function in the Schrödinger picture is obtained. Some statistical aspects of this model are presented. The results are employed to perform a careful investigation of the temporal evolution of the atomic inversion, entropy squeezing and variance squeezing. General conclusions reached are illustrated by numerical results.

Keywords Pair coherent states · Sub-Poissonian distribution · Pegg and Barnett formalism · W-function and Q-function · Cauchy-Schwarz inequalities

A.-S.F. Obada · E.M. Khalil
Mathematics Department, Faculty of Science, Al-Azhar University, Nasr City 11884, Cairo, Egypt

A.-S.F. Obada
e-mail: asobada@yahoo.com

E.M. Khalil (✉)
e-mail: eiedkhalil@yahoo.com

1 Introduction

Quantum entanglement is considered to be basic prerequisite for teleportation of quantum state, quantum communication, quantum computing, quantum information processing and testing quantum mechanics experimentally [1–7]. Theoretical and experimental studies on quantum communication through the use of nonlocal correction of entangled states have shown great promise for establishing new kinds of information processing with no classical counterparts [1]. One example is the concept of quantum teleportation [4], where as an entangled state was built from two single-mode phase squeezed vacuum states combined at a beam splitter [2]. Other examples of the application of entanglement to communications include dense coding [7] and quantum cryptographe [3]. These extensive studies have paved a way towards a variety of useful quantum informational devices.

Information theory cannot be separated from its physical representation, it is always to be stored in some physical systems, manipulated by some physical processes. This observation has a number of consequences for information theory. Perhaps, the most striking one is that, it makes a big difference whether the information is stored and processed in classical or quantum mechanical systems [8–11]. Until now this has always been done using systems governed by classical physics, e.g., one bit of information in a system that could take either of two states [12–15]. In a quantum computer information would be stored in quantum mechanical two-state systems, so-called qubits. The most peculiar feature of a qubit (and all quantum systems) is the existence of superpositions: according to the superposition principle (experimentally well established), a qubit, which can be in two distinct physical states can also be in an arbitrary coherent superposition of these states, representing in a certain sense both numbers at the same time. Moreover, the superposition principle is the basis for the quantum phenomenon of entanglement which is of particular importance for quantum communication. The study of entanglement has turned into a very fruitful field of research, revealing many strange features of quantum mechanics. Various types of entanglement have been discovered [16–18].

It is important to point out that the increased insight into the nonclassical properties of quantum states, they play a significant role in various physical applications. For instance, multimode entangled states serve as necessary resources in multiuser quantum communication network (see, e.g., [19–21]). Many new types of nonclassical states have been designed [22] according to the fundamental principles of quantum optics. Coherent states, their variants and generalizations have been extensively studied over the last four decades. A comprehensive review of this development can be found in Refs. [23, 24]. Subsequently the notion was generalized in various ways. Motivations to generalize the concept have arisen from symmetry considerations [25], dynamics [26] and algebraic aspects [27]. A generalized class of the conventional coherent state, called the nonlinear coherent states or the f-coherent states [28–31], has been constructed.

Pair coherent states (PCS) are regarded as an important type of correlated two-mode states, which possess prominent nonclassical properties. Such states denoted by $|\zeta, q\rangle$ are eigenstates of the operator $(\hat{a}\hat{b})$ and the number difference $(\hat{n}_a - \hat{n}_b)$ where $\hat{a}$ and $\hat{b}$ are the annihilation operators of the field modes and $\hat{n}_a = \hat{a}^\dagger\hat{a}$ and $\hat{n}_b = \hat{b}^\dagger\hat{b}$. These states satisfy

$$\hat{a}\hat{b}|\zeta, q\rangle = \zeta|\zeta, q\rangle \quad \text{and} \quad (\hat{n}_a - \hat{n}_b)|\zeta, q\rangle = q|\zeta, q\rangle. \tag{1}$$

The experimental realization of such nonclassical states is of practical importance. Agarwal [32–35] suggested that the optical (PCS) can be generated via the competition of 4-wave mixing and two-photon absorption in a nonlinear medium. Another scheme has been suggested for generating vibrational pair coherent states via the quantized motion of a trapped

ion in a two-dimensional trap [36]. In addition to various kinds of known nonclassical states [37, 38], a new one called a trio coherent state (TCS) has been introduced [39–43]. These states have been investigated and the even and odd trio coherent states have been studied for antibunching and Cauchy-Schwarz inequalities [42].

It is important to point out that the increased insight into the dynamics of the two-level systems (JCM) model [43]. It is has been generalized in many different ways. One such way is the multiphoton generalization [44] described by the following Hamiltonian ($\hbar = 1$),

$$H = \omega a^{\dagger} a + \frac{\omega_0}{2} S_z + \lambda \big(S_{12} a^k + a^{\dagger k} S_{21} \big), \tag{2}$$

where k is a positive integer and represents the multiplicity of the photons, λ is the coupling constant, ω_0 and ω are the atomic transition frequency and resonant mode frequency respectively. The annihilation (creation) operator $a(a^{\dagger})$ of the field mode for which the commutation relation $[a, a^{\dagger}] = 1$ is satisfied, while the operators S_{ij} are the generators of the $SU(2)$ group with they satisfy the commutation relation $[S_{ij}, S_{kl}] = S_{il}\delta_{jk} - S_{ki}\delta_{li}$ and $S_z = S_{11} - S_{22}$. There are a huge number of papers that appeared in the literature considering this model in great detail. Most of these papers concentrate on statistical aspects as well as the dynamics of the model. However, to meet the experimental realization, there are several attempts to generalize and modify this model [44]. For instance, the consideration of multimode and multiphoton appears in [45, 46] instead of single mode and single photon. In modeling typical experiments one considers a three-level atomic system interacting with two laser fields [47, 48] and reduces it to a two-level problem on the assumption of large detunings by using the adiabatic elimination [49]: the effective Hamiltonian obtained in this way has the form of the usual Jaynes-Cummings model. Adiabatic elimination has been criticized on several grounds [50–53], however, other methods of deriving effective Hamiltonians exist [54–57].

The aim of this paper is to review some recent work on *Entangled finite dimensional pair coherent states* and the theoretical investigations and of the experimental observations concerning the dynamical features of these states related dynamical systems. The physical situations which we shall refer to, belong to the experimental domains of cavity quantum electrodynamics and of trapped ion physics. The relative simplicity of the ion-trap model and the ease with which it can be extended through analytic expressions or numerical computation continue to attract attention. The physical scenario relative to the problems we shall face involves two trapped ions interacting with a laser field. The work reported here is originally motivated by several connections between quantum entanglement states and quantum information theory.

2 Finite Dimensional Pair Coherent States

In contrast to the pair coherent state finite dimensional PCS is defined as the eigenstate of the pair operator $(\hat{a}^{\dagger}\hat{b} + \frac{\zeta^{q+1}(\hat{a}\hat{b}^{\dagger})^q}{(q!)^2})$ for the two modes, and the sum of the photon number operators for the two modes $(\hat{a}^{\dagger}\hat{a} + \hat{b}^{\dagger}\hat{b})$, namely:

$$\begin{aligned} \left(\hat{a}^{\dagger}\hat{b} + \frac{\zeta^{q+1}(\hat{a}\hat{b}^{\dagger})^q}{(q!)^2} \right) |\zeta, q\rangle_F &= \zeta |\zeta, q\rangle_F, \\ \big(\hat{a}^{\dagger}\hat{a} + \hat{b}^{\dagger}\hat{b}\big) |\zeta, q\rangle_F &= q |\zeta, q\rangle_F, \end{aligned} \tag{3}$$

where the parameter ζ is a complex variable while the parameter q is non-negative integer number. The state takes the form,

$$|\zeta, q\rangle_F = N_q \sum_{n=0}^{q} \zeta^n \sqrt{\frac{(q-n)!}{q!n!}} |q-n, n\rangle, \tag{4}$$

in the two mode states $|n_a, n_b\rangle = |n_a\rangle \otimes |n_b\rangle$, where $|n_s\rangle$ is the Fock state for the mode s ($s = a$ or b) and the normalization constant N_q is given by

$$N_q = \left[\sum_{n=0}^{q} |\zeta|^{2n} \frac{(q-n)!}{q!n!} \right]^{\frac{-1}{2}} = \left({}_1F_0\left(-q, -|\zeta|^2\right) \right)^{\frac{-1}{2}}, \tag{5}$$

where ${}_1F_0$ is a generalized hypergeometric function. Because of the appearance of the operators $\hat{a}^\dagger \hat{b}$ or $\hat{a}\hat{b}^\dagger$ in this form and the finite sum it may be legitimate to call it a finite dimensional pair coherent state.

In what follows we address the problem of constructing and discussing some properties of these correlated two mode states of (4). The results that we are going to present stem from a new approach to the above state. Subsequently we shall examine the sub-Poissonian distribution and the phase properties of these states.

2.1 Generation Scheme

In this section we are concerned with the context of ion trap. Since ions can be trapped very efficiently and their entanglement with the environment is extremely weak, trapped ions have advantages for many purposes such as preparing various types of nonclassical states (see e.g. [58–64]), simulating nonlinear interactions [65], demonstrating quantum phase transitions [66, 67], establishing quantum search algorithms [68] and so on. The most promising merit of trapped ion systems is perhaps the possibility to implement scalable quantum computers [69] in which a number of ions are involved [70–72]. Nevertheless, many tasks can still be done even with a single ion. For instance, a controlled-NOT quantum logic gate can be performed just by a single trapped ion [73–76]. Here we propose an experimental scheme to generate the state of (4) in the vibronic motion of an ion which is trapped in real two-dimensional (2D) space.

The specification of the functions $(\hat{a}^\dagger \hat{b} + \frac{\zeta^{q+1}(\hat{a}\hat{b}^\dagger)^q}{(q!)^2})$ is subject to the generation schemes within the framework of the motion of a trapped ion in a 2-dimensional harmonic potential. Consider a single ion trapped in a 2-dimensional harmonic potential with frequencies ν_1 (in the x-direction), ν_2 (in the y-direction) in interaction with three laser fields propagating in the same direction tuned respectively to the electronic transition ω_0 of the ion and to the vibrational side band of frequency taken as follows: The first vibrational side band has the frequency $(\nu_2 - \nu_1)$ lower than that transition, but the second vibrational side band has the frequency q $(\nu_1 - \nu_2)$ higher than that transition. The Hamiltonian of this system is written as

$$\begin{aligned} H = {} & \nu_1 \hat{a}^\dagger \hat{a} + \nu_2 \hat{b}^\dagger \hat{b} + \frac{\omega_0}{2} \hat{\sigma}_z \\ & + \underline{\mu}.\Big[\Big\{ \underline{E_0} e^{i(k_1 \hat{x} + k_2 \hat{y} - \omega_0 t + \phi_0)} + \underline{E_1} e^{i(k_1 \hat{x} + k_2 \hat{y} - [\omega_0 - (\nu_2 - \nu_1)]t + \phi_1)} \\ & + \underline{E_2} e^{i(k_1 x + k_2 y - [\omega_0 - q(\nu_1 - \nu_2)]t + \phi_2)} \Big\} \hat{\sigma}_+ + h.c. \Big]. \end{aligned} \tag{6}$$

We denote by $\hat{a}$ and $\hat{b}$ the annihilation operators of the quantized bosons that describe the vibrational motion of the center of mass of trapped ion in the two dimensions x and y. The operators $\hat{\sigma}_+(\hat{\sigma}_-)$ and $\hat{\sigma}_z$ are the raising (lowering) and the population inversion operators of the electronic two-level ion which satisfy $[\hat{\sigma}_+, \hat{\sigma}_-] = \hat{\sigma}_z$, $[\hat{\sigma}_z, \hat{\sigma}_\pm] = \pm 2\hat{\sigma}_\pm$. $\underline{\mu}$ is the dipole matrix element and k_s $(s = 1, 2)$ are the components of the wave vectors of the driving laser fields of amplitudes E_0, E_1 and E_2. The quantized center-of-mass position $\hat{x}$ and $\hat{y}$ can be written as

$$\hat{x} = \Delta x\big(\hat{a} + \hat{a}^\dagger\big), \qquad \hat{y} = \Delta y\big(\hat{b} + \hat{b}^\dagger\big), \tag{7}$$

with Δx and Δy are the standard deviation for $\hat{x}$ and $\hat{y}$ in the ground state of the harmonic potential. We may use a vibrational rotating wave approximation and neglect the terms with fast oscillations [36, 77]. Thus the interactions Hamiltonian is simplified to

$$\begin{aligned} H_{\text{int}} = \exp\left[-\frac{(\eta_1^2+\eta_2^2)}{2}\right]\Bigg[\sigma_+\Bigg\{&\Omega_0\exp(i\phi_0)\sum_{m_1,m_2}\frac{(i\eta_1)^{2m_1}(i\eta_2)^{2m_2}}{(m_1!)^2(m_2!)^2}\hat{a}^{\dagger m_1}\hat{a}^{m_1}\hat{b}^{\dagger m_2}\hat{b}^{m_2} \\ &+\Omega_1\exp(i\phi_1)\sum_{m_1,m_2}\frac{(i\eta_1)^{2m_1+1}(i\eta_2)^{2m_2+1}}{m_1!(m_1+1)!m_2!(m_2+1)!}\hat{a}^{\dagger m_1+1}\hat{a}^{m_1}\hat{b}^{\dagger m_2}\hat{b}^{m_2+1} \\ &+\Omega_2\exp(i\phi_2)\sum_{m_1,m_2}\frac{(i\eta_1)^{2m_1+q}(i\eta_2)^{2m_2+q}}{m_1!(m_1+q)!m_2!(m_2+q)!}\hat{a}^{\dagger m_1}\hat{a}^{m_1+q}\hat{b}^{\dagger m_2+q}\hat{b}^{m_2}\Bigg\} + h.c.\Bigg]. \end{aligned} \tag{8}$$

$|\Omega_0| = |\underline{\mu}.\underline{E_0}|$, $|\Omega_1| = |\underline{\mu}.\underline{E_1}|$ and $|\Omega_2| = |\underline{\mu}.\underline{E_2}|$ are the Rabi frequencies related to the different laser fields and η_s are the Lamb-Dicke parameters, where $\eta_1 = k_1\Delta x$, $\eta_2 = k_2\Delta y$ [11]. It should be noted that $\hat{n}_1 + \hat{n}_2$ is a constant of motion for the Hamiltonian (8). The terms between parenthesis in (8) can be treated as follows: In the Lamb-Dicke limit where the vibrational amplitude of the ions is much smaller than the laser wavelength where it is sufficient to keep the first term in each series appearing in (8) and thus (8) is simplified to

$$H_{\text{int}} = \lambda\left(\hat{a}^\dagger\hat{b} + \frac{\zeta^{q+1}(\hat{a}\hat{b}^\dagger)^q}{(q!)^2} - \zeta\right)\hat{\sigma}_+ + h.c., \tag{9}$$

where $\lambda = -\Omega_1\eta_1\eta_2\exp[-\frac{(\eta_1^2+\eta_2^2)}{2} + i\phi_1]$ and $\zeta = \frac{\Omega_0\exp i(\phi_0-\phi_1)}{\Omega_1\eta_1\eta_2}$, while Ω_2 is related to the other parameters through the formula $\Omega_2 = \frac{\zeta^{q+1}\Omega_1}{(-1)^{q-1}(\eta_1\eta_2)^{q-1}}$. Therefore the parameters ζ and q are controlled by the amplitudes and phases of the applied laser fields and the Lamb-Dicke parameters. In the experiments performed on $^9Be^+$ ion with laser beam containing $\approx 1\ nw$ of power at 313 nm, the Lamb-Dicke parameter η is calculated to be ≈ 0.23. Thus using this estimate for η_1 and η_2 puts $\eta_1\eta_2 \approx 0.05$. For the values $|\zeta| \approx \eta_1\eta_2$ and for arbitrary q, then $\Omega_0 \sim \Omega_2 \sim \Omega_1(\eta_1\eta_2)^2$ which gives $\Omega_0 \sim \Omega_2 \sim \frac{\Omega_1}{400}$. Thus the value for E_1 has to be two orders of magnitude higher than E_0 and E_2. Since $\Omega_i = \underline{\mu}.\underline{E_i} = \mu\ E_i\cos(\theta_i)$ $(i = 0, 1, 2)$ the angle θ_i can be used to reduce the estimate for E_i. This means that moderate values for E_0 and E_2 and strong value of E_1 are sufficient to produce such state with arbitrary q for $|\zeta| \approx \eta_1\eta_2$. However for larger values of $|\zeta|$ then the number q has to be restricted to reasonable values for appropriate laser fields.

The master equation for the density matrix under spontaneous emission with energy dissipation rate γ is given by [36]

$$\frac{\partial\hat{\rho}}{\partial t} = -i[\hat{H}_{\rm int}, \hat{\rho}] + \frac{\gamma}{2}[2\hat{\sigma}_-\hat{\rho}\hat{\sigma}_+ - \hat{\sigma}_+\hat{\sigma}_-\hat{\rho} - \hat{\rho}\hat{\sigma}_+\hat{\sigma}_-]. \tag{10}$$

The stationary solution $\hat{\rho}_s$ for this master equation is obtained by setting $\frac{\partial\bar{\rho}}{\partial t} = 0$. A solution $\hat{\rho}_s$ can be given as

$$\hat{\rho}_s = |g\rangle|\zeta\rangle\langle\zeta|\langle g|, \tag{11}$$

with $|g\rangle$ the electronic ground state ($\hat{\sigma}_-|g\rangle = 0, \langle g|\hat{\sigma}_+ = 0$) and $|\zeta\rangle$ is the vibration eigenstate that satisfies $\hat{H}_{\rm int}|\zeta\rangle = 0$. It is straightforward to show that $|\zeta\rangle$ belongs to the class of states considered in (4). To tailor the Hamiltonian of any nonlinear multi-quanta JCM a scheme of using a number of lasers has been presented to produce such interaction [78, 79]. It is to be mentioned that the nonlinear JCM has been realized experimentally [80, 81].

2.2 Relations to Other States

2.2.1 Relation to SU(2) Group

The Schwinger angular-momentum operators [82] are defined as

$$\hat{J}_x = \frac{(\hat{a}^\dagger\hat{b} + \hat{b}^\dagger\hat{a})}{2}, \qquad \hat{J}_y = \frac{(\hat{a}^\dagger\hat{b} - \hat{b}^\dagger\hat{a})}{2i}, \qquad \hat{J}_z = \frac{(\hat{a}^\dagger\hat{a} - \hat{b}^\dagger\hat{b})}{2} \tag{12}$$

which are the generators of the Lie algebra of $SU(2)$ and satisfy $[\hat{J}_x, \hat{J}_y] = i\hat{J}_z$, $[\hat{J}_y, \hat{J}_z] = i\hat{J}_x$ and $[\hat{J}_z, \hat{J}_x] = i\hat{J}_y$. It is useful to introduce the following operators

$$\hat{J}_+ = \hat{J}_x + i\hat{J}_y = \hat{a}^\dagger\hat{b}, \qquad \hat{J}_- = \hat{J}_x - i\hat{J}_y = \hat{a}\hat{b}^\dagger. \tag{13}$$

Furthermore, the operator

$$\hat{C}_2 = \hat{J}_z^2 + \frac{1}{2}(\hat{J}_+\hat{J}_- + \hat{J}_-\hat{J}_+) \tag{14}$$

which is just the square of the total angular momentum, commutes with all the generators of the Lie algebra. The unitary irreducible representations of the $SU(2)$ are just the familiar angular momentum states $|j, m\rangle$ satisfying the relations

$$\begin{aligned} &\hat{C}_2|j,m\rangle = j(j+1)|j,m\rangle, \qquad J_z|j,m\rangle = m|j,m\rangle, \\ &\hat{J}_\pm|j,m\rangle = \sqrt{(j\mp m)(j\pm m+1)}|j,m\pm1\rangle, \quad j = \frac{1}{2}, 1, \frac{3}{2}, 2, \ldots, \\ &\qquad\qquad\qquad\qquad\qquad\qquad\qquad\qquad m = -j, -j+1, \ldots, j. \end{aligned} \tag{15}$$

Note that the representations are finite dimensional, the dimension for a given j being $2j+1$. Now we solve the following equation

$$\left(\hat{J}_- + \frac{\zeta^{2j+1}}{((2j)!)^2}(\hat{J}_+)^{2j}\right)|\zeta\rangle = \zeta|\zeta\rangle \tag{16}$$

which leads to in this is the same form of (4) when we label $q = 2j$ and identify the states $\{|j, m-j\rangle\}$ as the states $\{|q-n, n\rangle\}$.

2.2.2 Exponential Form

The state $|\zeta, q\rangle$ of (4) may be cast as

$$|\zeta, q\rangle_F = N_q \sum_{s=0}^{q} \zeta^n \frac{(q-s)!\hat{a}^s \hat{b}^{\dagger s}}{q!s!}|q, 0\rangle. \tag{17}$$

One can show that

$$\left[g(\hat{n}_a, \hat{n}_b)\hat{a}\hat{b}^\dagger\right]^s = \hat{a}^s \hat{b}^{\dagger s} \prod_{m=1}^{s} g(\hat{n}_a - m, \hat{n}_b + m). \tag{18}$$

Here $g(\hat{n}_a, \hat{n}_b)$ is an arbitrary function of $\hat{n}_a$ and $\hat{n}_b$. Then using (18) with $g(\hat{n}_a, \hat{n}_b) = \frac{\zeta}{(\hat{n}_a+1)}$, the state $|\zeta, q\rangle$ is finally written in the exponential form

$$|\zeta, q\rangle_F = N_q \sum_{s=0}^{\infty} \frac{[\frac{\zeta}{(\hat{n}_a+1)}\hat{a}\hat{b}^\dagger]^s}{s!}|q, 0\rangle = N_q \exp\left[\frac{\zeta}{(\hat{n}_a+1)}\hat{a}\hat{b}^\dagger\right]|q, 0\rangle.$$

2.3 Nonclassical Effects

The experimental feasibility of models involving more than one mode multi-mode in a high-Q cavity has been more or less considered by many authors [83–86]. It is worthwhile remarking that investigating such models goes beyond an intrinsic theoretical interest because a new generation of high-Q electromagnetic cavities, covering a wide wave-length range, are today realizable [83–87]. Thus, in the following subsections we will investigate the influence of the controlling parameters q on the nonclassical behavior of the cavity field where, in particular, the sub-Poissonian distribution and the phase distribution are emphasized.

2.3.1 Sub-Poissonian Distribution

We devote the following discussion to consider an example of the nonclassical effect that is the phenomenon of sub-Poissonian distribution. This phenomenon can be measured by photon detectors based on photoelectric effect. It is well known that, sub-Poissonian statistics is characterized by the fact that the variance of the photon number $\langle(\Delta\hat{n}_i)^2\rangle$ is less than the average photon number $\langle\hat{a}_i^\dagger\hat{a}_i\rangle = \langle\hat{n}_i\rangle$. This can be expressed by means of the normalized second-order correlation function for the mode z in a quantum state $|\zeta, q\rangle_F$ [88, 89] as follows:

$$g_z^{(2)}(\zeta) = \frac{{}_F\langle\zeta, q|\hat{n}_z(\hat{n}_z - 1)|\zeta, q\rangle_F}{{}_F\langle\zeta, q|\hat{n}_z|\zeta, q\rangle_F^2}, \quad \forall z = a, b, \tag{19}$$

where

$$\begin{aligned} {}_F\langle\zeta, q|\hat{n}_a(\hat{n}_a - 1)|\zeta, q\rangle_F &= N_q^2 \sum_{n=0}^{q} \frac{|\zeta|^{2(n)}(q-n)!}{q!n!}(q-n)(q-n-1), \\ {}_F\langle\zeta, q|\hat{n}_b(\hat{n}_b - 1)|\zeta, q\rangle_F &= N_q^2 \sum_{n=0}^{q} \frac{|\zeta|^{2(n)}(q-n)!}{q!n!}n(n-1), \end{aligned} \tag{20}$$

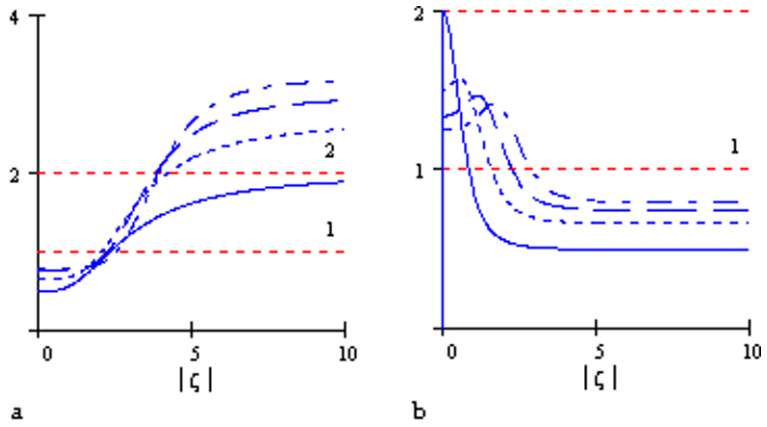

Fig. 1 The sub-Poissonian function as a function of $|\zeta|$, (**a**) for mode a, (**b**) for mode b, where the *solid curve* for $q=2$, the *dot curve* for $q=3$, the *dash curve* for $q=4$ and the *dashdot curve* for $q=5$

and

$$
\begin{aligned}
{}_F\langle\zeta,q|\hat{n}_a|\zeta,q\rangle_F &= N_q^2\sum_{n=0}^{q}\frac{|\zeta|^{2n}(q-n)!}{n!}(q-n),\\
{}_F\langle\zeta,q|\hat{n}_b|\zeta,q\rangle_F &= N_q^2\sum_{n=0}^{q}\frac{|\zeta|^{2n}(q-n)!}{n!}n.
\end{aligned}
\tag{21}
$$

The function $g_z^{(2)}(\zeta)$ given by (19) for the mode z serves as a measure of the deviation from the Poissonian distribution that corresponds to coherent states with $g_z^{(2)}(\zeta)=1$. If $g_z^{(2)}(\zeta)<1$ (>1), the distribution is called sub (super)-Poissonian, if $g_z^{(2)}(\zeta)=2$ the distribution is called thermal and when $g_z^{(2)}(\zeta)>2$ it is called super-thermal.

To reveal the physical content of the state, we plot $g_a^{(2)}(\zeta)$ against $|\zeta|$. First when we take $q=0$ or 1 the function $g_a^{(2)}(\zeta)=0$ due to the fact that the states present are either vacuum or one photon and for both of them $g^{(2)}(\zeta)$ is zero. For the effectiveness we take $q=2$ it is to be observed that the state starts at $g_a^{(2)}(0)=0.5$ and for a short interval of $|\zeta|$ the function $g_a^{(2)}(\zeta)$ has full sub-Poissonian distribution. Also super-Poissonian behavior appears for higher values of ζ and its behavior almost like the thermal distribution as observed in Fig. 1(a). In Fig. 1(a) we take $q=3,4,5$, we find that the function starts at $\frac{2}{3}$, $\frac{3}{4}$ and $\frac{4}{5}$ respectively. This is because it looks as that we have the Fock state $|q\rangle$ present in this case when $\zeta\to 0$ and $g_a^{(2)}(\zeta)=\frac{q-1}{q}$. In this basis, we see that $g_a^{(2)}(\zeta)<1$ for a short range of ζ. When the parameter ζ is increased further, the state $|\zeta,q\rangle$ exhibits super-Poissonian behavior and for large values of $|\zeta|$ the state reaches super-thermal state behavior because for $\zeta\to\infty$ we get these limit $g_b^{(2)}(\zeta)=\frac{4(q-1)}{q}$. The nonclassical nature of the state is apparent, when one takes the value $q=2$ the function $g_a^{(2)}(\zeta)<1$ as shown in Fig. 1(a), but when we take $q>2$ the function $g_a^{(2)}(\zeta)>2$ for higher values of ζ.

To simplify the visual comparison we finally consider the function $g_b^{(2)}(\zeta)$ for the second mode. In this case q takes the values 2, 3, 4 and 5 we find that the function $g_b^{(2)}(\zeta)$ starts at 2, $\frac{3}{2}$, $\frac{4}{3}$ and $\frac{5}{4}$ respectively. Because of the condition between the two modes, thus when we take the limits as $\zeta\to 0$ we get these limit $g_b^{(2)}(\zeta)=\frac{q}{q-1}$. We see that $g_b^{(2)}(\zeta)$ has a decreasing trend and so for sufficiently large values of $|\zeta|$ it shows sub-Poissonian behavior because for

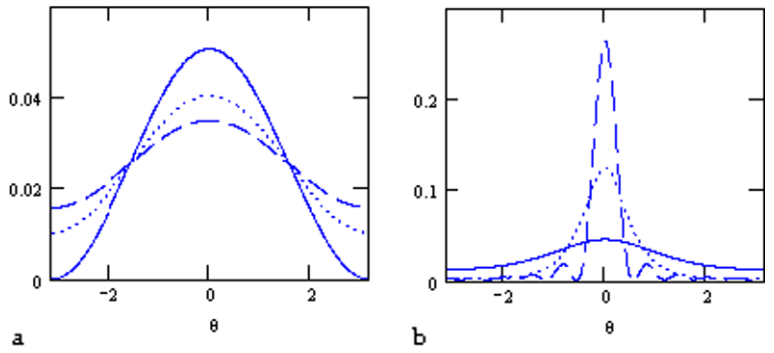

Fig. 2 The phase distribution $P_{\zeta,q}(\theta_1,\theta_2)$ against the angle $\theta=(\theta_2-\theta_1)$, (**a**) $q=1$, (**b**) $q=10$, where the *solid curve* for $\zeta=1$, the *dot curve* for $\zeta=3$ and the *dash curve* for $\zeta=5$

$\zeta\to\infty$ we get these limit $g_b^{(2)}(\zeta)=\frac{q-1}{q}$. For further increase of q the state $|\zeta,q\rangle$ exhibits full sub-Poissonian behavior (see Fig. 1(b)). We note that the super-Poissonian distribution interval increases by increasing the parameter q. As it is exhibited by Figs. 1(a, b) the modes a and b behave differently for small values of ζ and also for large values of ζ. However, both modes may show sub-Poissonian behavior. For example, when we take $\zeta=\sqrt{2}$ and $q=2$ it is found that $g_a^{(2)}(\zeta)=g_b^{(2)}(\zeta)=\frac{2}{3}$ which means sub-Poissonian behavior in both modes.

2.3.2 Phase Properties

In the present section we shall discuss the phase distribution for the finite dimensional pair coherent states. For this reason it is convenient to use the phase distribution formalism introduced by Barnett and Pegg [88–95]. It is well known that the phase operator is defined as the projection operator on a particular phase state multiplied by the corresponding value of the phase. Therefore one can find that the Pegg-Barnett phases distribution function $P_{\zeta,q}(\theta_1,\theta_2)$ is given by [93–95]:

$$P_{\zeta,q}(\theta_1,\theta_2)=\frac{|N_q|^2}{(2\pi)^2}\sum_{n,m}\zeta^n\zeta^{*m}\sqrt{\frac{(q-n)!(q-m)!}{q!n!q!m!}}\times\exp\big[i\big[(q-n)-(q-m)\big]\theta_1+i(n-m)\theta_2\big]. \tag{22}$$

Therefore the phases distribution function can be written as

$$P_{\zeta,q}(\theta_1,\theta_2)=\frac{|N_q|^2}{(2\pi)^2}\left|\sum_n\zeta^n\sqrt{\frac{(q-n)!}{q!n!}}\exp[in\theta]\right|^2,\quad -\pi\le\theta\le\pi, \tag{23}$$

which is normalized according to $\int_{-\pi}^{\pi}\int_{-\pi}^{\pi}P(\theta_1,\theta_2,\zeta)\,d\theta_1\,d\theta_2=1$. Due to the correlated between the two modes, the phase distribution depends on the difference between the phases of the modes. In Fig. 2 we plot $P_{\zeta,q}(\theta)$ against the angle $\theta=\theta_2-\theta_1$ for different valued of the parameter q and $|\zeta|$.

Generally for very small (large) values of $|\zeta|$ the state (4) almost represents a Fock state and hence the information about the phase is lost. As $|\zeta|$ increases partial coherent phase states result and the phase distribution shows a peak. This peak is centered at $\theta=0$ and the

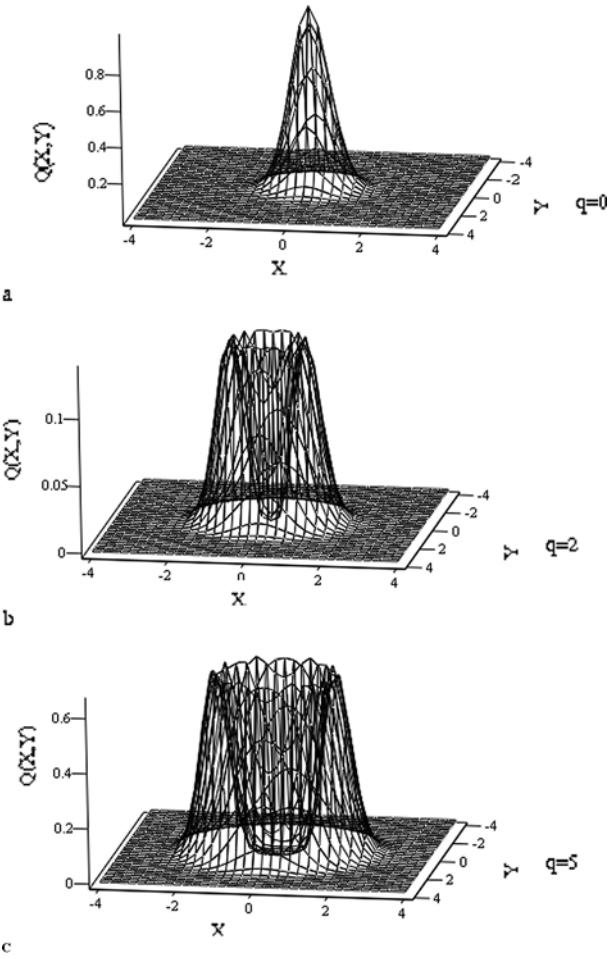

Fig. 3 The $Q(x, y)$ as function of (x, y). (**a**) $q = 0$, (**b**) $q = 2$, (**c**) $q = 5$

distribution is symmetric around this peak. For $q = 1$, plotted in Fig. 2(a) it is observed that $P_{\zeta,q}(\theta)$ starts at $P_{\zeta,q}(-\pi) = 0, 0.01, 0.016$ when $|\zeta| = 1, 3, 5$ respectively. The maxima for the distribution at $\theta = 0$ decrease by increasing $|\zeta| = 1$. In Fig. 2(b) we take a large value for the parameter q ($q = 10$) and the same values of $|\zeta|(1, 3, 5)$. We see that the function $P_{\zeta,q}(\theta)$ starts at $P(-\pi) = 0.013, 0.002, 0.003$ when $|\zeta| = 1, 3, 5$ respectively. The maxima for the distribution at $\theta = 0$ by increasing the value of $|\zeta|$. However, this increase turns to a decrease for larger values of $|\zeta|$. The maximum value for $P_{\zeta,q}(0)$ shifts to higher values of $|\zeta|$ as q increases.

2.3.3 Q-function

It has been shown from earlier studies [96–98] that the quasi-probability (Wigner-Moyal W-, Husimi-Kano Q- and Glauber-Sudarshan P-) function, are important for the statistical description of a microscopic system and provide insight into the non-classical features of the radiation fields. In this section we shall concentrate on the Q- and W-functions only.

For that purpose we consider the two-mode Q-function defined as

$$Q(\alpha,\beta)=\frac{1}{\pi^2}\big|\langle\alpha,\beta|\zeta,q\rangle\big|^2, \tag{24}$$

where $\alpha,\beta\in C$ and $|\alpha,\beta\rangle=|\alpha\rangle|\beta\rangle$, with $|\alpha\rangle$ and $|\beta\rangle$ the usual coherent states. Generally there are four variables associated with the real and imaginary parts of α,β. For visualization let us confine ourselves to a subspace determined by $\alpha=\beta$ [68]. In that subspace the Q-function for the finite dimensional pair coherent state is calculated to be

$$Q(x,y)=\frac{\exp[-2(x^2+y^2)]}{\pi^2}\left|N_q\sum_{n=0}^{q}\frac{\zeta^n\alpha^q}{\sqrt{q!n!}}\right|^2, \tag{25}$$

where $x=Re(\alpha)$ and $y=Im(\alpha)$. We can write the effective function as a function of $r=\sqrt{x^2+y^2}$

$$Q(r)\sim r^q\exp\big[-2r^2\big]. \tag{26}$$

The maximization or minimization depend on the parameter q, when $q=0$ there exist unique maximum value at $r=0$. For $q>0$ there exist maximization at $r=\sqrt{q}$ and minimization at $r=0$.

We represent in Fig. 3 the function $Q(r)$ we take different values for q. We find that when $q=0$ the function $Q(r)$ for the state $|\zeta,0\rangle$ has one peak centered at $r=0$, as shown in Fig. 3(a) and the distribution is almost Gaussian for the vacuum state. For the $|\zeta,2\rangle$, the shape of the function is sensitive to changes in q (Figs. 3(b) and 3(c)) where the state $|\zeta,q\rangle$ is the most effective state and contribution is the mainly effective one where a crater is apparent in the center. However, if we increase q the center crater-like spreads out in the phase space and the diameter increases as the q increase as shown in Fig. 3(c).

3 Superposition of the Finite Dimensional Pair Coherent State

The correlated two-mode states $|\zeta,q,\phi\rangle$ are defined as superposition of two finite dimensional state separated in phase by π.

$$|\zeta,q,\phi\rangle=N_\phi\big[|\zeta,q\rangle+\exp(i\phi)|-\zeta,q\rangle\big], \tag{27}$$

where the normalization constant N_ϕ is given by

$$N_\phi=\frac{1}{\sqrt{2}}\left[1+N_q^2\cos\phi\sum_{n=0}^{q}(-1)^n|\zeta|^{2n}\frac{(q-n)!}{q!n!}\right]^{-\frac{1}{2}}. \tag{28}$$

It is easy to verify that the states $|\zeta,q,\phi\rangle$ are eigenstates of the operator $(\hat{a}^\dagger\hat{b}+\frac{\zeta^{q+1}(\hat{a}\hat{b}^\dagger)^q}{(q!)^2})^2$ with eigenvalue ζ^2. In this contribution we focus on the two special cases of ϕ (namely $\phi=0$ and π), the general form can be rewritten as follows:

$$\begin{aligned}|\zeta,q\rangle_j&=N_{q,j}^2\sum_{n=0}^{[\frac{q-j}{2}]}\zeta^{2n+j}\sqrt{\frac{(q-2n-j)!}{q!(2n+j)!}}|q-2n-j,2n+j\rangle,\\ N_{q,j}^{-2}&=\sum_{n=0}^{[\frac{q-j}{2}]}|\zeta|^{4n+2j}\frac{(q-2n-j)!}{q!(2n+j)!},\quad j=0,1.\end{aligned} \tag{29}$$

Now we discuss some statistical properties of these correlated two mode states of (29). The results that we are going to present stem from a new approach to the superposing of the finite dimensional states. Subsequently we shall examine the sub-Poissonian distribution, The behavior of the phase distribution in the framework of Pegg and Barnett formalism and the Wigner function the Q-function of the state (29) are discussed.

3.1 Sub-Poissonian Distribution

In the present section we consider an example of the nonclassical effects that is the phenomenon of sub-Poissonian distribution. This can be expressed by means of the normalized second-order correlation function in (19). Where

$$
\begin{aligned}
{}_j\langle\zeta,q|\hat{n}_a(\hat{n}_a-1)|\zeta,q\rangle_j &= N_{q,j}^2\sum_{n=0}^{[\frac{q-j}{2}]}\frac{|\zeta|^{4n+2j}(q-2n-j)!}{q!(2n+j)!}(q-2n-j)(q-2n-j-1),\\
{}_j\langle\zeta,q|\hat{n}_b(\hat{n}_b-1)|\zeta,q\rangle_j &= N_{q,j}^2\sum_{n=0}^{\frac{q-j}{2}}\frac{|\zeta|^{4n+2j}(q-2n-j)!}{q!(2n+j)!}(2n+j)(2n+j-1),
\end{aligned}
\tag{30}
$$

and

$$
\begin{aligned}
{}_j\langle\zeta,q|\hat{n}_a|\zeta,q\rangle_j &= N_{q,j}^2\sum_{n=0}^{[\frac{q-j}{2}]}\frac{|\zeta|^{4n+2j}(q-2n-j)!}{q!(2n+j)!}(q-2n-j),\\
{}_j\langle\zeta,q|\hat{n}_b|\zeta,q\rangle_j &= N_{q,j}^2\sum_{n=0}^{[\frac{q-j}{2}]}\frac{|\zeta|^{4n+2j}(q-2n-j)!}{q!(2n+j)!}(2n+j).
\end{aligned}
\tag{31}
$$

The function $g_z^{(2)}(\zeta)$ given by (19) for the mode z serves as a measure of the deviation from the Poissonian distribution that corresponds, as we mentioned before, to coherent states with $g_z^{(2)}(\zeta)=1$. If $g_z^{(2)}(\zeta)<1$ (>1), the distribution is called sub (super)-Poissonian, if $g_z^{(2)}(\zeta)=2$ the distribution is called thermal and when $g_z^{(2)}(\zeta)>2$ it is called super-thermal.

In Fig. 4(a), the second-order correlation function $g_a^{(2)}(\zeta)$ given by (19), (30), (31) for q taking odd numbers is plotted against $|\zeta|$ for $q=3,5,7$ there exist two cases. The first case when we take $j=0$, this figure exhibits the very striking quantum nature of the generated field. For the first mode, we find that the distribution function starts to be sub-Poissonian $g_a^{(2)}(0)<1$ at small values of $|\zeta|$ which starts from $\frac{q-1}{q}$, but by increasing the parameter q the function $g_a^{(2)}(\zeta)$ reaches a super-Poissonian distribution $(g_a^{(2)}(\zeta)>1)$ as appearing in Fig. 4(a). For the second mode at some value of $|\zeta|$ the state with $j=0$ becomes super-thermal $(g_b^{(2)}(0)>2)$ while the state with higher values of ζ the distribution becomes sub-Poissonian. Thus when we take the limits as $\zeta\to\infty$ we get these limit $g_b^{(2)}(\zeta)=\frac{q}{q-1}$ see Fig. 4(b).

The second case when we take $j=1$. In this case we find larger changes occurring in the shape of the curve for the function $g_a^{(2)}(\zeta)$. For the first mode the function $g_a^{(2)}(\zeta)$ starts with sub-Poissonian distribution. For higher values of $|\zeta|$ the function $g_a^{(2)}(\zeta)$ becomes super-Poissonian and super-thermal as observed in Fig. 5(a). For the second mode the function $g_b^{(2)}(\zeta)$ starts from 0, by increasing of the parameter $|\zeta|$ the function reaches to super-Poissonian see Fig. 5(b). Increasing of $|\zeta|$ makes the distribution returns to sub-Poissonian distribution. The limits as $\zeta\to\infty$ equal $g_b^{(2)}(\zeta)=\frac{q-1}{q}$.

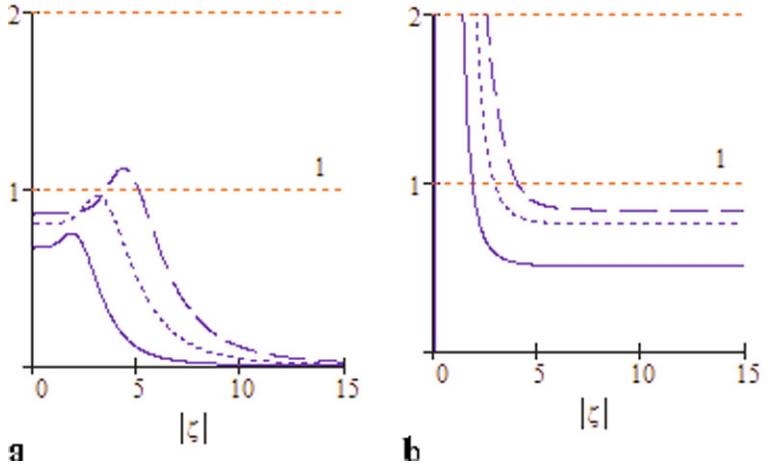

Fig. 4 The second-order function of $|\zeta|$, $j = 0$. (**a**) For mode a, (**b**) for mode b, where the *solid curve* for $q = 3$, the *dotted curve* for $q = 5$ and the *dashed curve* for $q = 7$

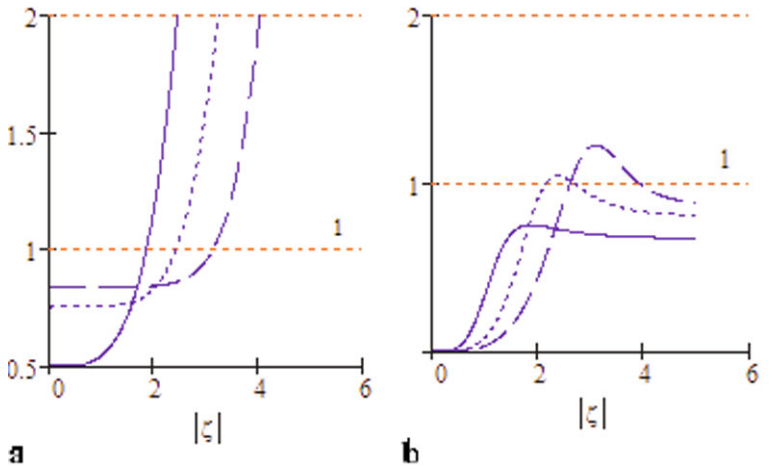

Fig. 5 Same as Fig. 4 but $j = 1$

When q takes even numbers, for the first and the second modes when $(j = 0, 1)$ the behavior is the same as the above case when $(j = 1, 0)$ respectively, for the other parameters fixed.

The cross correlation between the two-mode is given by

$$\Delta_{\text{cross}}(\zeta) = {}_j\langle\zeta, q|\hat{n}_a\hat{n}_b|\zeta, q\rangle_j - {}_j\langle\zeta, q|\hat{n}_a|\zeta, q\rangle_{jj}\langle\zeta, q|\hat{n}_b|\zeta, q\rangle_j.$$

If Δ_{cross} is a positive quantity, this means that the modes are correlated, while anti-correlation amongst the modes occurs when Δ_{cross} is negative values. In Fig. 6 the cross correlation function $\Delta_{\text{cross}}(\zeta)$ is plotted against $|\zeta|$ for $q = 3, 5, 7$. From the figure the function $\Delta_{\text{cross}}(\zeta)$ negative and the nonclassicality behavior is demonstrated by increase of the parameter q.

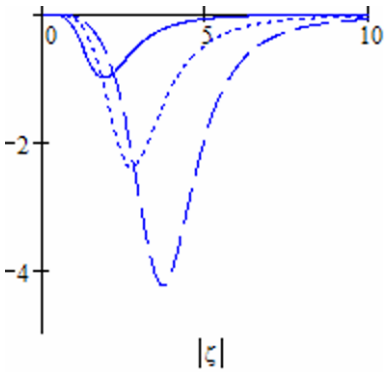

Fig. 6 The cross correlation between the two-mode as a function of $|\zeta|$, $j = 0$ where the *solid curve* for $q = 3$, the *dotted curve* for $q = 5$ and the *dashed curve* for $q = 7$

3.2 Cauchy-Schwarz Inequality Violation

The Cauchy-Schwarz inequality is defined as

$$ {}_j\langle\zeta, q|\hat{n}_a(\hat{n}_a - 1)|\zeta, q\rangle_j\, {}_j\langle\zeta, q|\hat{n}_b(\hat{n}_b - 1)|\zeta, q\rangle_j \geq {}_j\langle\zeta, q|\hat{n}_a\hat{n}_b|\zeta, q\rangle_j^2. \tag{32} $$

We shall examine the scaled Cauchy-Schwarz inequalities in the superposition of the finite dimensional PCS determined by

$$ F_{ab}(\zeta) = \frac{{}_j\langle\zeta, q|\hat{n}_a(\hat{n}_a - 1)|\zeta, q\rangle_j\, {}_j\langle\zeta, q|\hat{n}_b(\hat{n}_b - 1)|\zeta, q\rangle_j}{{}_j\langle\zeta, q|\hat{n}_a\hat{n}_b|\zeta, q\rangle_j^2}. \tag{33} $$

The inequality (32) is violated if the function F_{ab} is less than unity. For that purpose we need to calculate the expectation values appearing in (30). Those in the numerator were already known from (33) and those in the denominator are calculated to be generally for $j = 0, 1$.

$$ {}_j\langle\zeta, q|\hat{n}_a\hat{n}_b|\zeta, q\rangle_j = N_{q,j}^2 \sum_{n=0}^{[\frac{q-j}{2}]} \frac{|\zeta|^{4n+2j}(q-2n-j)!}{q!(2n+j)!}(q-2n-j)(2n+j). \tag{34} $$

The Cauchy-Schwarz inequality for the finite dimensional pair coherent state is clearly seen in Fig. 7 for the two modes (a, b). Where $q = 3, 5, 7$ and for case $j = 0$, partial violation starting from non-zero for short interval of $|\zeta|$ and full violated after short interval (a partial violation means that $F_{23} > 1$ at small $|\zeta|$ and then becomes less than unity for large $|\zeta|$). As the parameter $|\zeta|$ increases the function $F_{ab}(\zeta)$ reaches zero as in Fig. 7(a). For $j = 1$ full violation starting from zero, after short interval the function $F_{ab}(\zeta)$ becomes partially violated as observed in Fig. 7(b). The second case when q takes even number namely $(q = 4, 6, 8)$. For $j = 0$ we see that all curves do not suffer violation and they never reach unity see Fig. 8(a). While for $j = 1$ the function $F_{ab}(\zeta)$ shows full violation starting from zero, as the parameter $|\zeta|$ progresses the function $F_{ab}(\zeta)$ shows partial variolation. After short interval the behavior returns to full violation and the function $F_{ab}(\zeta)$ reaches zero as observed in Fig. 8(b). The violation is stronger (weaker) at small $|\zeta|$ (large $|\zeta|$)-region. However, the variolation depends on the parameter q for small values of q the function $F_{ab}(\zeta)$ almost less than unity. But for larger values of q the function $F_{ab}(\zeta)$ shows partial violation.

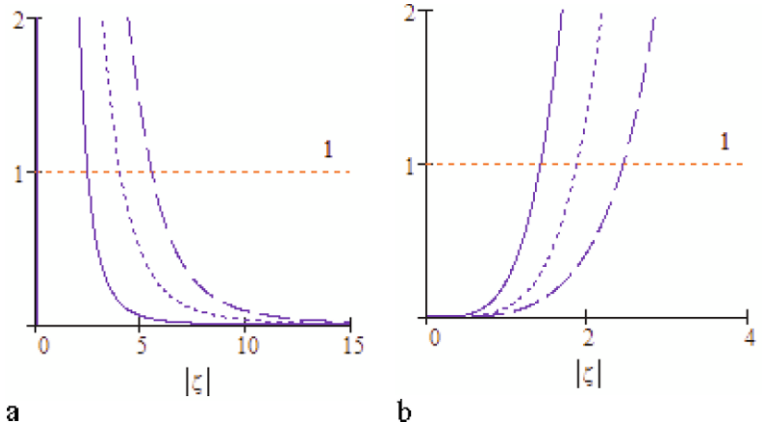

Fig. 7 F_{ab} as a function of $|\zeta|$, (**a**) for fixed $j = 0$ and the *solid curve* for $q = 3$, the *dotted curve* for $q = 5$ and the *dashed curve* for $q = 7$, (**b**) same as (**a**) but $j = 1$

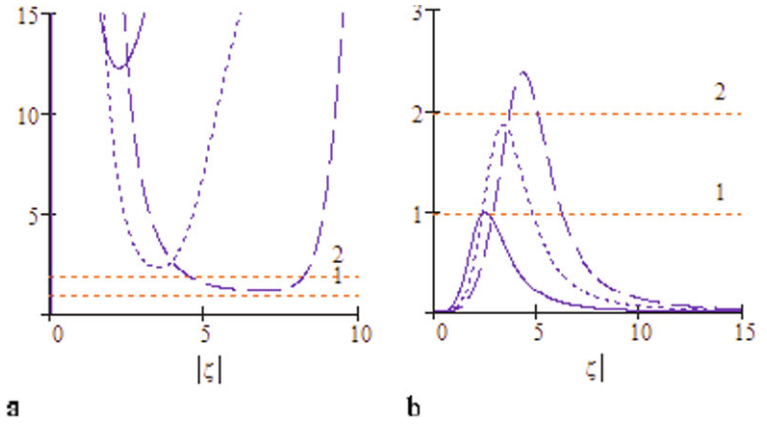

Fig. 8 Same as Fig. 3 but the *solid curve* for $q = 4$, the *dotted curve* for $q = 6$ and the *dashed curve* for $q = 8$

3.3 Phase Properties

It is well known that the phase operator is defined as the projection operator on a particular phase state multiplied by the corresponding value of the phase. Therefore one can find that the Pegg-Barnett phase distribution function $P_{\zeta,q}(\theta_1, \theta_2)$ is given by [93–95]:

$$P_{\zeta,q}(\theta_1,\theta_2) = \frac{|N_q|^2}{(2\pi)^2} \sum_{n,m} \zeta^{2n+j} \zeta^{*2m+j} \sqrt{\frac{(q-2n-j)!(q-2m-j)!}{q!(2n+j)!q!(2m+j)!}}$$
$$\times \exp\big[i\big[(q-2n-j)-(q-2m-j)\big]\theta_1 + i(2n-2m)\theta_2\big]. \quad (35)$$

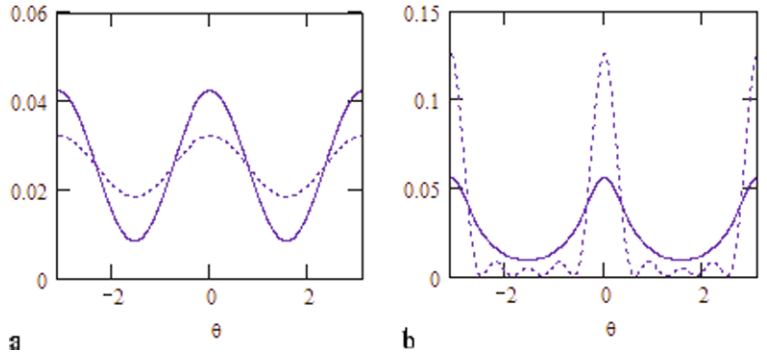

Fig. 9 The phase distribution $P(\theta)$ as a function of θ and (**a**) $j=0$, the *solid curve* for $\zeta=3$ and the *dotted curve* for $\zeta=5$, (**b**) same as (**a**) but $j=1$

Therefore the phases distribution function can be written as

$$P_{\zeta,q}(\theta_1,\theta_2)=\frac{|N_q|^2}{(2\pi)^2}\left|\sum_n \zeta^{2n+j}\sqrt{\frac{(q-2n-j)!}{q!(2n+j)!}}\exp[i2n\theta]\right|^2,\quad -\pi\leq\theta\leq\pi, \tag{36}$$

with $\theta=\theta_2-\theta_1$. Due to the correction between the two modes, the phase distribution depends on the difference between the phases of the two modes. In the figures we plot $P_{\zeta,q}(\theta)$ against the angle $\theta=\theta_2-\theta_1$ for different values of the parameter q and $|\zeta|$.

Generally for very small (large) values of $|\zeta|$ the state (27) almost represents a Fock state and hence the information about the phase is lost. As $|\zeta|$ increases partial coherent phase states result and the phase distribution shows a thee-peak structure. The model peak is centered at $\theta=0$ and the distribution is symmetric around the central peak and has wings at $\theta=\pm\pi$. For $q=3$, plotted in Fig. 9(a), it is observed that $P_{\zeta,q}(\theta)$ starts at $P_{\zeta,q}(-\pi)=0.042, 0.032$ when $|\zeta|=3,5$ respectively. The maxima for the distribution at $\theta=0$ decrease by increasing $|\zeta|$. In Fig. 9(b) we take a large value for the parameter q $(q=10)$ and the same values of $|\zeta|$ (3, 5). We see that the function $P_{\zeta,q}(\theta)$ starts at $P(-\pi)=0.056$, (0.125) when $|\zeta|=3$, (5) respectively. The maxima for the distribution.at $\theta=0$ by increasing the value of $|\zeta|$. In Fig. 9(b) we take larger values for the parameter q $(q=10)$ and the same values of $|\zeta|$ (3, 5). We see that the function $P_{\zeta,q}(\theta)$ starts at $P_{\zeta,q}(\theta)=0.056$, (0.125) when $|\zeta|=3$, (5) respectively. The maxima of the phase distribution are increased by increasing of the parameter $|\zeta|$ (see Fig. 9b). However this increase turns to a decrease for larger values of $|\zeta|$. The maximum value for $P_{\zeta,q}(0)$ shifts to higher values of $|\zeta|$ as q increases.

3.4 s-Parameterized Quasiprobability Function (QDF)

The QDF's for a quantum state of a physical system are useful tools for investigating the dynamical and statistical properties of a quantum mechanical system [96–115]. They include the Glauber-Sudarshan P-function [101], the Wigner W-function [97, 98] and the Husimi Q-function [102, 103] which are closely related to the operator ordering in the mathematical description of a physical system.

The s-parameterized characteristic function (CF) is perhaps one of the most well-known important function in quantum optics, since it is the Fourier transform of the s-parameterized

QDF. The s-parameterized CF for a single-mode field is defined by [107, 108]

$$C(\lambda,s)=Tr\big[\hat{\rho}\hat{D}(\lambda)\big]\exp\left(\frac{s}{2}|\lambda|^2\right), \tag{37}$$

with $\hat{D}(\lambda)$ is the displacement operator given by $\hat{D}(\lambda)=\exp(\lambda\hat{a}^+-\lambda^*\hat{a})$, and $\lambda=|\lambda|e^{i\theta}$. Here, s is ordering parameter where $s=(-1)1$ means (anti-)normal ordering and $s=0$ is symmetrical or Weyl ordering [107, 108].

The s-parameterized quasi-probability function is the Fourier transform of the s-parameterized characteristic function

$$F(\beta,s)=\frac{1}{\pi^2}\int C(\lambda,s)\exp\big(\lambda^*\beta-\lambda\beta^*\big)\,d^2\lambda, \tag{38}$$

where the real parameter s defines the corresponding phase space distribution. As mentioned above it is associated with the ordering of the field bosonic operators.

Since the finite dimensional PCS (27) is a two-mode state, thus the definitions ((37) and (38)) have to be extended to two-mode case. The s-parameterized CF for the two-mode states is defined as follows

$$C(\lambda_1,\lambda_2,s)=Tr\big[\hat{\rho}\hat{D}(\lambda_1)\hat{D}(\lambda_2)\big]\exp\left\{\frac{s}{2}\big(|\lambda_1|^2+|\lambda_2|^2\big)\right\}. \tag{39}$$

Thus the s-parameterized QDF for the two-mode case is given by

$$F(\beta_1,\beta_2,s)=\left(\frac{1}{\pi^2}\right)^2\iint C(\lambda_1,\lambda_2,s)\exp\big(\lambda_1^*\beta_1+\lambda_2^*\beta_2-\lambda_1\beta_1^*-\lambda_2\beta_2^*\big)\,d^2\lambda_1\,d^2\lambda_2. \tag{40}$$

It is noted that formulae (39) and (40) are extensions of formulae (37) and (38) for CF and QDF of the single mode fields.We consider a phase space QDF for our states. To begin the state (27) will be written in the form

$$|\zeta,q\rangle_B=\sum_{n=0}^{[\frac{q-j}{2}]}B_n(\zeta,q)|q-2n-j,2n+j\rangle, \tag{41}$$

where

$$B_n(\zeta,q)=N_{q,j}^2\zeta^{2n+j}\sqrt{\frac{(q-2n-j)!}{q!(2n+j)!}}.$$

For the density operator $\hat{\rho}=|\zeta,q\rangle\langle q,\zeta|$ the s-parameterized CF has the two mode form, using (41) for the state (29) in the formulae (39) and (40), we get

$$\begin{aligned}C(\lambda_1,\lambda_2,s)=&\exp\left[\left\{-\frac{(1-s)}{2}\right\}\big(|\lambda_1|^2+|\lambda_2|^2\big)\right]\\&\times\sum_{n=0}^{[\frac{q-j}{2}]}\sum_{m=0}^{[\frac{q-j}{2}]}B_n(\zeta,q)B_m^*(\zeta,q)\sqrt{\frac{(q-2n-j)!}{(q-2m-j)!}}\\&\times\sqrt{\frac{(2n+j)!}{(2m+j)!}}L_{q-2n-j}^{2n-2m}\big[|\lambda_1|^2\big]L_{2n+j}^{2m-2n}\big[|\lambda_2|^2\big],\end{aligned} \tag{42}$$

where $L_m^n(x)$ are associated Laguerre polynomials given by

$$L_m^n(x) = \sum_{r=0}^{m} \binom{m+n}{m-r} \frac{(-1)^r}{r!} x^r, \tag{43}$$

$$\begin{aligned} F(\beta_1, \beta_2, s) = N_{q,j}^2 \left(\frac{2}{\pi(1-s)}\right)^2 \exp\left[\frac{-2(|\beta_1|^2 + |\beta_2|^2)}{(1-s)}\right] \\ \times \sum_{n=0}^{[\frac{q-j}{2}][\frac{q-j}{2}]} \sum_{m=0} \zeta^{2n+j} \zeta^{*2m+j} \frac{(q-2n-j)!}{(2m+j)!} \\ \times \left(\frac{1+s}{(1-s)}\right)^q L_{q-2n-j}^{2n-2m}\left[\frac{4|\beta_1|^2}{(1-s^2)}\right] L_{2n+j}^{2m-2n}\left[\frac{4|\beta_2|^2}{(1-s^2)}\right]. \end{aligned} \tag{44}$$

Note that in (42) and (44) there exist two associated Laguerre polynomials. For negative values of $(m-n)$ or $(n-m)$ we use the formula [116]

$$L_{n+\alpha}^{(-\alpha)}(z) = (-z)^\alpha \frac{n!}{(n+\alpha)!} L_n^{(\alpha)}(z).$$

For visualization of these functions let us confine ourselves to a subspace determined by $\alpha = \beta$ [68], we find that the s-parameterized QDF for our field states may be written in the following form:

$$\begin{aligned} F(\beta, s) = N_{q,j}^2 \left(\frac{2}{\pi(1-s)}\right)^2 \exp\left[\frac{-4(|\beta|^2)}{(1-s)}\right] \sum_{n=0}^{[\frac{q-j}{2}]} |\zeta|^{4n+2j} \frac{(q-2n-j)!}{(2n+j)!} \\ \times \left(\frac{1+s}{(1-s)}\right)^q L_{q-2n-j}^0\left[\frac{4|\beta|^2}{(1-s^2)}\right] L_{2n+j}^0\left[\frac{4|\beta|^2}{(1-s^2)}\right]. \end{aligned} \tag{45}$$

This formula gives the exact analytical expressions for the s-parameterized QDF for the state (29). It is noted that, for the P-function, i.e., $s = 1$, special attention has to be paid in performing the limit $s \to 1$ [117]. Originally the P function was introduced in an alternative way independently by Sudershan [99]. Recently, Wünsche discussed the nonclassicality of states defined by nonpositivity of the P-function [117]. However we shall not discuss this function here any further. Instead we concentrate on the other two quasi-probability functions namely Wigner and Q-functions.

In Fig. 10 we plot $W(\beta)$, i.e., $s = 0$ in (45) for $j = 1$, $\zeta = 5$, and $q = 4$ and 5. It is clear that (for q odd) the Wigner function has negative peak at the origin observed and oscillatory regime around the main peak. The non-classicality effect is more pronounced when q is odd. The spreading of Wigner function over the β-plane is shown as q increases. For the parameter q even, we can see the W function is almost positive and has Gaussian central peak which range surrounding it. We can see in general when q is even the W function has upward peak at the origin, while it has downward peak when q is odd at the origin. As shown in Fig. 10 the oscillatory behavior is clear for large values of q.

On the other hand, the Q function is positive definite for every point in the phase space. The Q-function for a single mode field can be written in a more compact form defined in (24). The function $Q(\beta)$ has been constructed in homodyne experiments [109, 110]. By

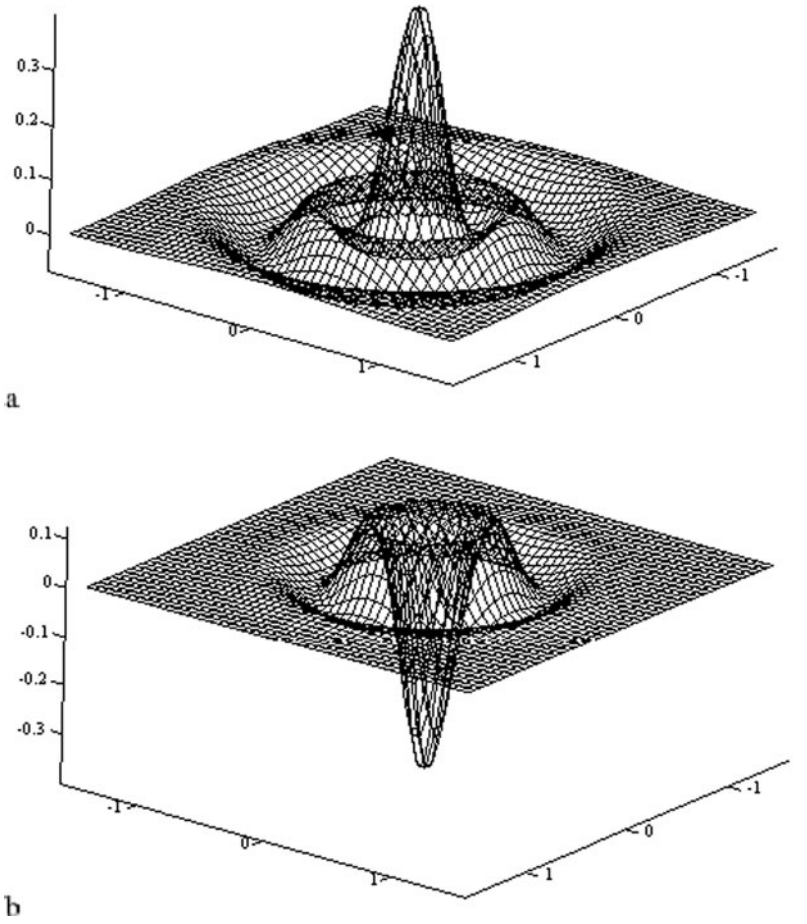

Fig. 10 The Wigner function as a function of (x, y), where $j = 1$, $\zeta = 5$, (**a**) $q = 4$, (**b**) $q = 5$

considering the properties of Q-function, the interference effects and photon number distribution in phase space can be discussed [115].

For that purpose we consider the two-mode Q-function in the form

$$Q(\alpha, \beta) = \frac{1}{\pi^2} |\langle \alpha, \beta | \zeta, q \rangle|^2, \tag{46}$$

where $\alpha, \beta \in \mathbb{C}$ and $|\alpha, \beta\rangle = |\alpha\rangle|\beta\rangle$, with $|\alpha\rangle$ and $|\beta\rangle$ the usual coherent states. Generally there are four variables associated with the real and imaginary parts of α, β. For visualization let us confine ourselves to a subspace determined by $\alpha = \beta$ [68]. It is obtained from (47) by written $(s = 1)$. In that subspace the Q-function for the state (27) is calculated to be

$$Q(x, y) = \frac{\exp[-2(x^2 + y^2)]}{\pi^2} \left| N_{q,j} \sum_{n=0}^{q} \frac{\zeta^{2n+j} \alpha^q}{\sqrt{q!}(2n + j)!} \right|^2, \tag{47}$$

where $x = Re(\alpha)$ and $y = Im(\alpha)$. We can write the effective function as a function of $r = \sqrt{x^2 + y^2}$ on the form $Q(x, y) = A_{q,j} f(r)$ where

$$f(r) = r^{2q} \exp\left[-2r^2\right]. \tag{48}$$

By comparing between (25), (26) and (48), (49) we see that same behavior, so the maximization or minimization depend on the parameter q. When $q = 0$ there exists unique maximum value at $r = 0$. For $q > 0$ there exists maxima at $r = \sqrt{\frac{q}{2}}$ and minima at $r = 0$ as mentioned after (25), (26).

4 Non-Linear Finite Dimensional Pair Coherent State

In the present section we develop the idea of the finite dimensional PCS by introduce a nonlinear finite dimensional state (NPCS) [116] as the eigenstate of the pair operators

$$\begin{aligned} &\left(f_1(\hat{n}_a)\hat{a}^\dagger f_2(\hat{n}_b)\hat{b} + \frac{\zeta^{q+1}(\hat{a}\frac{1}{f_1(\hat{n}_a)}\frac{1}{f_2(\hat{n}_b)}\hat{b}^\dagger)^q}{(q!)^2}\right) \quad \text{and} \\ &\hat{Q} = \left(\hat{a}^\dagger\hat{a} + \hat{b}^\dagger\hat{b}\right) \end{aligned} \tag{49}$$

for the two modes. Namely:

$$\begin{aligned} \left(f_1(\hat{n}_a)\hat{a}^\dagger\hat{b} f_2(\hat{n}_b) + \frac{\zeta^{q+1}(\hat{a}\frac{1}{f_1(\hat{n}_a)}\frac{1}{f_2(\hat{n}_b)}\hat{b}^\dagger)^q}{(q!)^2}\right)|\zeta, q\rangle &= \zeta|\zeta, q\rangle, \\ \hat{Q}|\zeta, q\rangle &= q|\zeta, q\rangle, \end{aligned} \tag{50}$$

where the parameter ζ is a complex variable while the parameter q is an integer. The expansion of this state in the two mode states $|n_a, n_b\rangle = |n_a\rangle \otimes |n_b\rangle$, where $|n_s\rangle$ is the Fock state for the mode s ($s = a$ or b) takes the form

$$|\zeta, q\rangle = N_q \sum_{n=0}^{q} \zeta^n \sqrt{\frac{(q-n)!}{q!n!}} \frac{f_1(q-n)!}{f_1(q)!f_2(n)!}|q-n, n\rangle, \tag{51}$$

where $f(n)! = f(0).\, f(1)\ldots f(n)$ and $f(0) = 1$ the normalization constant N_q is given by

$$N_q = \left[\sum_{n=0}^{q} |\zeta|^{2n} \frac{(q-n)!}{q!n!}\left(\frac{f_1(q-n)!}{f_1(q)!f_2(n)!}\right)^2\right]^{\frac{-1}{2}}. \tag{52}$$

Because of the appearance of the operators $\hat{a}^\dagger\hat{b}$ or $\hat{a}\hat{b}^\dagger$ in this form and the functions $f_1(\hat{n}_a)$ and $f_2(\hat{n}_b)$ it may be legitimate to call it a finite dimensional nonlinear pair coherent state, or converter state. Once we have introduced this class of nonlinear finite dimensional pair coherent state, we wish to discuss some of their statistical properties. The results that we are going to present are concerned with the examination of the sub-Poissonian distribution and the phase properties of the state obtained. But before we do this, a generation scheme for the mentioned state is demonstrated in the next section.

4.1 Generation Scheme

Here we propose an experimental scheme to generate the state of (51) in the vibrionic motion of an ion which is trapped in real two-dimensional (2D) space. The specification of the operators $(f_1(\hat{n}_a)\hat{a}^\dagger f_2(\hat{n}_b)\hat{b} + \frac{\zeta^{q+1}(\hat{a}\frac{1}{f_1(\hat{n}_a)}\frac{1}{f_2(\hat{n}_b)}\hat{b}^\dagger)^q}{(q!)^2})$ is subject to the generation schemes within the framework of the motion of a trapped ion in a 2-dimensional harmonic potential. Consider a single ion trapped in a 2-D harmonic potential with frequencies ν_1 (in the x-direction), ν_2 (in the y-direction) in interaction with three laser fields propagating in the same direction tuned respectively to the electronic transition ω_0 of the ion and to the vibrational side band of frequency taken as follows: The first vibrational side band has the frequency $(\nu_2 - \nu_1)$ lower than that transition, but the second vibrational side band has the frequency $q(\nu_2 - \nu_1)$ higher than that transition. The Hamiltonian of this system is written as (6). As before use a vibrational rotating wave approximation and neglect the terms with fast oscillations. Thus the interactions Hamiltonian is simplified to that approximating in (8) before. It should be noted that $\hat{n}_1 + \hat{n}_2$ is a constant of motion for the Hamiltonian (8). The terms between parenthesis in (8) can be summed in terms of the associated Laguerre polynomials thus instead of (9) a generalized form is given as follows:

$$H_{\text{int}} = \lambda\big(f_1(\hat{n}_a)\hat{a}^\dagger f_2(\hat{n}_b)\hat{b} + \zeta^{q+1}\hat{a}^q f_3(\hat{n}_a)\hat{b}^{\dagger q} f_4(\hat{n}_b) - \zeta\big)\sigma_+ + h.c., \tag{53}$$

where

$$f_1(\hat{n}_a) = \frac{L^1_{\hat{n}_a-1}(\eta_1^2)}{(\hat{n}_a)L^0_{\hat{n}_a}(\eta_1^2)}, \qquad f_2(\hat{n}_b) = \frac{L^1_{\hat{n}_b}(\eta_2^2)}{(\hat{n}_b+1)L^0_{\hat{n}_b}(\eta_2^2)},$$
$$f_3(\hat{n}_1) = \frac{(\hat{n}_a - q)!L^1_{\hat{n}_a-q}(\eta_1^2)}{(\hat{n}_a)!L^0_{\hat{n}_a}(\eta_1^2)}, \qquad f_4(\hat{n}_b) = \frac{\hat{n}_b!L^1_{\hat{n}_b}(\eta_2^2)}{(\hat{n}_b+q)!L^0_{\hat{n}_b+q}(\eta_2^2)}, \tag{54}$$

$$\lambda = -\Omega_1\eta_1\eta_2 L^0_{\hat{n}_a}\big(\eta_1^2\big)L^0_{\hat{n}_b}\big(\eta_2^2\big)\exp\Big[-\frac{(\eta_1^2+\eta_2^2)}{2} + i\phi_1\Big], \tag{55}$$

where ζ same as (9) and $L_n^m(x)$ is the associated Laguerre polynomials given by (43). While Ω_2 is related to the other parameters through the formula

$$\Omega_2 = \frac{\zeta^{q+1}\Omega_1}{(-1)^{q-1}(\eta_1\eta_2)^{q-1}f_1(q)!f_2(q)!}. \tag{56}$$

Therefore the parameters ζ and q are controlled by the amplitudes and phases of the applied laser fields and the Lamb-Dicke parameters. As has been mentioned before the experimental evidences lead to estimation of the Lamb-Dicke parameter η is calculated to be ≈ 0.23. Thus using this estimate for η_1 and η_2 puts $\eta_1\eta_2 \approx 0.05$. For the values $|\zeta| \approx \eta_1\eta_2$ and for arbitrary q, then $\Omega_0 \sim \Omega_1(\eta_1\eta_2)^2$, $\Omega_2 \sim \Omega_1\frac{(\eta_1\eta_2)^2}{f_1(q)!f_2(q)!}$ which gives $\Omega_0 \sim \frac{\Omega_1}{400}$ $\Omega_2 \sim \frac{\Omega_1}{400f_1(q)!f_2(q)!}$. Thus the value for E_1 has to be two orders of magnitude higher than E_0 and E_2. Since $\Omega_i = \underline{\mu}.\underline{E_i} = \mu\ E_i\cos(\theta_i)$ $(i = 0, 1, 2)$ the angle θ_i can be used to reduce the estimate for E_i. This means that moderate values for E_0 and E_2 and strong value of E_1 are sufficient to produce such state with arbitrary q for $|\zeta| \approx \eta_1\eta_2$. However for larger values of $|\zeta|$ then the number q must attain large values for appropriate laser fields. For generating the state of (51) let us look at the master equation for the density matrix under spontaneous emission

with energy dissipation rate γ which is given by

$$\frac{\partial\bar{\rho}}{\partial t} = -i[H_{\rm int}, \rho] + \frac{\gamma}{2}[2\sigma_-\rho\sigma_+ - \sigma_+\sigma_-\rho - \rho\sigma_+\sigma_-]. \tag{57}$$

The stationary solution $\bar{\rho}_s$ for this master equation is obtained by setting $\frac{\partial\bar{\rho}}{\partial t} = 0$. A solution $\bar{\rho}_s$ can be given as

$$\bar{\rho}_s = |g\rangle|\zeta\rangle\langle\zeta|\langle g|, \tag{58}$$

with $|g\rangle$ the electronic ground state ($\sigma_-|g\rangle = 0, \langle g|\sigma_+ = 0$) and $|\zeta\rangle$ is the vibration eigenstate that satisfies $H_{\rm int}|\zeta\rangle = 0$. It is straightforward to show that $|\zeta\rangle$ belongs to the class of states considered in (51). To tailor the Hamiltonian of any nonlinear multi-quanta JCM a scheme of using a number of lasers has been presented to produce such interaction [78, 79]. It is to be mentioned that the nonlinear JCM has been realized experimentally [79] as mentioned earlier.

4.2 Relations to Other States

4.2.1 Relation to SU(2) Group

To relate the states (51), (52) to realizations of this group we use the operators J_x, J_y and J_z are defined as

$$\begin{aligned} J_x &= \frac{(f_1(\hat{n}_a)\hat{a}^\dagger f_2(\hat{n}_b)\hat{b} + \hat{a}\frac{1}{f_1(\hat{n}_a)}\hat{b}^\dagger\frac{1}{f_2(\hat{n}_b)})}{2}, \\ J_y &= \frac{(f_1(\hat{n}_a)\hat{a}^\dagger f_2(\hat{n}_b)\hat{b} - \hat{a}\frac{1}{f_1(\hat{n}_a)}\hat{b}^\dagger\frac{1}{f_2(\hat{n}_b)})}{2i}, \\ J_z &= \frac{(\hat{n}_a - \hat{n}_b)}{2} \end{aligned} \tag{59}$$

which satisfy the commutation relations $[J_x, J_y] = iJ_z$, $[J_y, J_z] = iJ_x$ and $[J_z, J_x] = iJ_y$. Note that neither J_x nor J_y is a hermitian operator, we get they satisfy the same $SU(2)$ conditions. It is useful to introduce the following operators

$$J_+ = J_x + iJ_y = f_1(\hat{n}_a)\hat{a}^\dagger f_2(\hat{n}_b)\hat{b}, \qquad J_- = J_x - iJ_y = \hat{a}\frac{1}{f_1(\hat{n}_a)}\hat{b}^\dagger\frac{1}{f_2(\hat{n}_b)}. \tag{60}$$

Note again that J_+ is not the hermitian conjugate of J_-. However, we have the commutation relation

$$[J_z, J_\pm] = \pm J_\pm, \qquad [J_+, J_-] = 2J_z. \tag{61}$$

Furthermore, the operator

$$\hat{C}_2 = J_z^2 + \frac{1}{2}(J_+J_- + J_-J_+) = \left(\frac{\hat{n}_a + \hat{n}_b}{2}\right)\left(\frac{\hat{n}_a + \hat{n}_b}{2} + 1\right). \tag{62}$$

These operators can be through of as operation under Lie algebra with the generators J_i. Once again we emphasis J_x and J_y are not hermitian operators and hence J_+ is not the hermitian conjugate of J_-. The operator $\hat{C}_2$ commutes with all the generators of the Lie algebra

and in the language of group theory is known as a Casimir operator. The state (52) is eigenstate for the operator $\hat{C}_2$ with eigenvalue $\frac{q}{2}(\frac{q}{2}+1)$. The unitary irreducible representations of the $SU(2)$ are just the familiar angular momentum states $|j,m\rangle$ satisfying the relations

$$\begin{aligned}
&\hat{C}_2|j,m\rangle = j(j+1)|j,m\rangle, \qquad J_z|j,m\rangle = m|j,m\rangle,\\
&J_+|j,m\rangle = \big|f_1(j+m+1)\big|\big|f_2(j-m-1)\big|\sqrt{(j+m+1)(j-m)}|j,m+1\rangle,\\
&J_-|j,m\rangle = \frac{\sqrt{(j+m)(j-m+1)}}{|f_1(j+m)||f_2(j-m)|}|j,m-1\rangle,\\
&\quad j = \frac{1}{2},1,\frac{3}{2},2,\ldots,\ m=-j,-j+1,\ldots,j.
\end{aligned} \tag{63}$$

Note that the representations are finite dimensional, the dimension for a given j being $2j+1$. Now if we take $q=2j$ the state (51) the result same as the linear case see (2.2.1) take the following form

$$\begin{aligned}
|\zeta,2j\rangle &= N_{2j}\sum_{n=0}^{2j}\zeta^n\frac{f_1(2j-n)!}{f_1(2j)!f_2(n)!}\sqrt{\frac{(2j-n)!}{2j!n!}}|2j-n,n\rangle\\
&= N_{2j}\sum_{n=-j}^{j}\zeta^{n+j}\frac{f_1(j-n)!}{f_1(2j)!f_2(n+j)!}\sqrt{\frac{(j-n)!}{2j!(n+j)!}}|j-n,n+j\rangle,
\end{aligned} \tag{64}$$

which is eigenstate of the operator $\hat{C}_2$ with eigenvalue $j(j+1)$.

4.2.2 Exponential Form

In a similar way to Sect. 2.2.2, we note that the state $|\zeta,q\rangle$ of (51) may be cast as

$$|\zeta,q\rangle = N_q\sum_{n=0}^{q}\zeta^n\frac{(q-n)!\hat{a}^n\hat{b}^{\dagger n}}{q!n!}\frac{f_1(q-n)!}{f_1(q)!f_2(n)!}|q,0\rangle. \tag{65}$$

One use (18) with

$$g(\hat{n}_a,\hat{n}_b) = \frac{\zeta}{f_1(\hat{n}_a)f_2(\hat{n}_b)\hat{n}_a}, \tag{66}$$

the state $|\zeta,q\rangle$ is finally written in the exponential form

$$|\zeta,q\rangle = N_q\sum_{n=0}^{\infty}\frac{[\hat{a}\hat{b}^\dagger\frac{\zeta}{f_1(\hat{n}_a)f_2(\hat{n}_b)\hat{n}_a}]^n}{n!}|q,0\rangle = N_q\exp\left[\hat{a}\hat{b}^\dagger\frac{\zeta}{f_1(\hat{n}_a)f_2(\hat{n}_b)\hat{n}_a}\right]|q,0\rangle \tag{67}$$

in a similar expression for the conventional coherent state. However, the representation of the coherent operator by the pair operator $\hat{a}\hat{b}^\dagger\frac{\zeta}{f_1(\hat{n}_a)f_2(\hat{n}_b)\hat{n}_a}$.

4.2.3 Bell States

Entanglement is an essential resource for many applications in quantum information science such as quantum superdense coding [118, 119] quantum teleportation [120–125], quantum cryptography [116–128] and quantum computing [129, 130] most of these applications are

based on the maximally-entangled two-particle quantum states called Bell states. The maximally entangled states are composed form single-phonon number states as $|\psi\rangle = |1,0\rangle$ or $|0,1\rangle$, two-phonon number state as $|\psi\rangle = |1,1\rangle$ and null-photon state as $|\psi\rangle = |0,0\rangle$. We can generate the maximally entangled states by taking the nonlinear functions $f_1(\hat{n}_a) = \hat{I}$ and $f_2(\hat{n}_b) = \hat{I}$ and the parameter q taken the values 1, 2, 0 respectively.

$$
\begin{aligned}
|1,1\rangle &= \frac{1}{\zeta N_2\sqrt{2}}\big[|\zeta,2\rangle - |-\zeta,2\rangle\big],\\
|0,1\rangle &= \frac{1}{2\zeta N_1}\big[|\zeta,1\rangle - |-\zeta,1\rangle\big],\\
|1,0\rangle &= \frac{1}{2N_1}\big[|\zeta,1\rangle + |-\zeta,1\rangle\big],\\
|0,0\rangle &= |0,0\rangle,
\end{aligned}
\tag{68}
$$

where N_q given by (52), the maximal entangled states are define as following

$$
\begin{aligned}
\psi_{\pm} &= \frac{1}{\sqrt{2}}\big(|1,1\rangle \pm |0,0\rangle\big),\\
\varphi_{\pm} &= \frac{1}{\sqrt{2}}\big(|1,0\rangle \pm |0,1\rangle\big).
\end{aligned}
\tag{69}
$$

Thus the maximally entangled states $\psi_{\pm}$, $\varphi_{\pm}$ which play an important role in quantum measurement theory, can be constructed from the states $|\zeta,q\rangle$.

4.3 Nonclassical Effects

In the following subsections we investigate the influence of the controlling parameters q, η_1 and η_2 on the nonclassical behavior of the modes where, in particular, the sub-Poissonian distribution and the phase distribution are discussed.

4.3.1 Sub-Poissonian Distribution

In this section, we shall evaluate the correlation function, to discuss the phenomenon of sub-Poissonian distribution for non-linear finite dimensional pair coherent state. This can be expressed by means of the normalized second-order correlation function (19) for the mode z in a quantum state $|\zeta,q\rangle$ as defined by (51) namely:

$$
g_z^{(2)}(\zeta) = \frac{\langle\zeta,q|\hat{n}_z(\hat{n}_z-1)|\zeta,q\rangle}{\langle\zeta,q|\hat{n}_z|\zeta,q\rangle^2}, \quad \forall z = a,b,
\tag{70}
$$

where

$$
\begin{aligned}
\langle\zeta,q|\hat{n}_a(\hat{n}_a-1)|\zeta,q\rangle &= N_q^2\sum_{n=0}^{q}|\zeta|^{2n}\left(\frac{f_1(q-n)!}{f_1(q)!f_2(n)!}\right)^2\frac{(q-n)!}{q!n!}(q-n)(q-n-1),\\
\langle\zeta,q|\hat{n}_b(\hat{n}_b-1)|\zeta,q\rangle &= N_q^2\sum_{n=0}^{q}|\zeta|^{2n}\left(\frac{f_1(q-n)!}{f_1(q)!f_2(n)!}\right)^2\frac{(q-n)!}{q!n!}n(n-1),
\end{aligned}
\tag{71}
$$

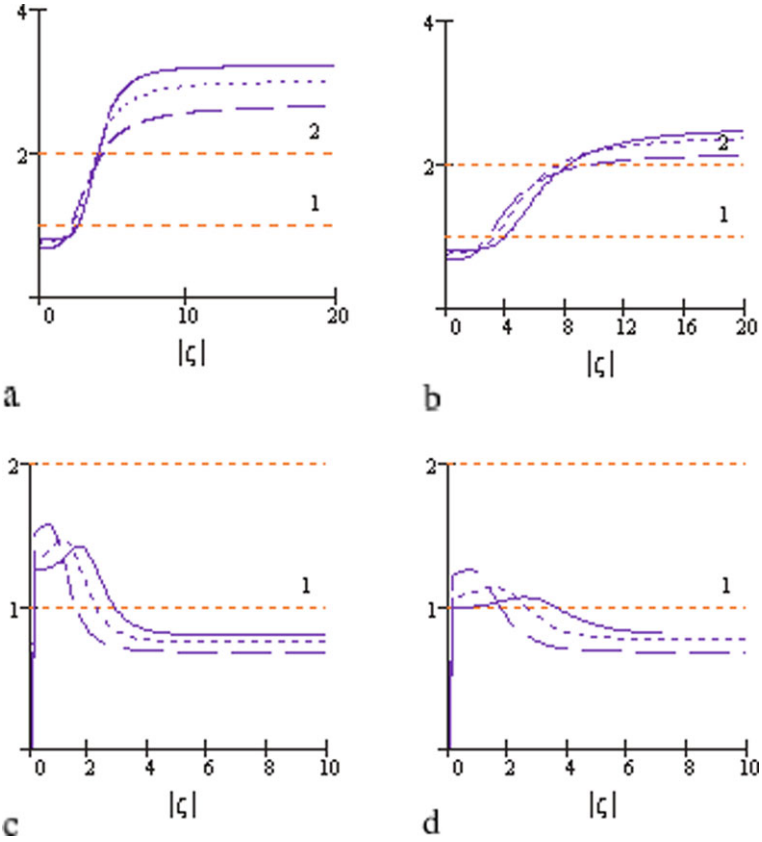

Fig. 11 The sub-Poissonian function as function of $|\zeta|$, (**a**) for mode a and $\eta = 0$, (**b**) for mode b and $\eta = 0$, (**c**) for mode a and $\eta = 0.3$, (**d**) for mode b and $\eta = 0.3$, where the *solid curve* for $q = 3$, the *dot curve* for $q = 4$, the *dash curve* for $q = 5$

and

$$\begin{aligned}\langle\zeta, q|\hat{n}_a|\zeta, q\rangle &= N_q^2 \sum_{n=0}^{q} |\zeta|^{2n} \left(\frac{f_1(q-n)!}{f_1(q)!f_2(n)!}\right)^2 \frac{(q-n)!}{n!}(q-n),\\ \langle\zeta, q|\hat{n}_b|\zeta, q\rangle &= N_q^2 \sum_{n=0}^{q} |\zeta|^{2n} \left(\frac{f_1(q-n)!}{f_1(q)!f_2(n)!}\right)^2 \frac{(q-n)!}{n!}n,\end{aligned} \tag{72}$$

where $f_1(q-n)$ and $f_2(n)$ are given by (55). The function $g_z^{(2)}(\zeta)$ for the mode z serves as a measure of the deviation from the Poissonian distribution that corresponds to coherent states with $g_z^{(2)}(\zeta) = 1$.

To reveal the physical content of the state, we plot $g_a^{(2)}(\zeta)$ against $|\zeta|$. The first case when we take $\eta = 0$, we show that when $q = 0$ or 1 the function $g_a^{(2)}(\zeta) = 0$ due to the fact that the states present are either vacuum or one photon and for both of them $g^{(2)}(\zeta)$ is zero. For the effectiveness we take $q = 3$ it is to be observed that the state starts at $g_a^{(2)}(0) = \frac{2}{3}$ and for a short interval of $|\zeta|$ the function $g_a^{(2)}(\zeta)$ has full sub-Poissonian distribution. Also super-Poissonian behavior appears for higher values of ζ and its behavior almost like the thermal

distribution as observed in Fig. 11(a). In Fig. 11(a) we take $q = 4, 5$, we find that the function starts at $\frac{3}{4}$ and $\frac{4}{5}$ respectively, as has been earlier studied in [100]. This is because it looks as that we have the Fock state $|q\rangle$ present in this case when $\zeta \to 0$ and $g_a^{(2)}(\zeta) = \frac{q-1}{q}$. In this basis, we see that $g_a^{(2)}(\zeta) < 1$ for a short range of ζ. When the parameter ζ is increased further, the state $|\zeta, q\rangle$ exhibits super-Poissonian behavior and for large values of $|\zeta|$ the state reaches super-thermal state behavior because for $\zeta \to \infty$ we get these limit $g_b^{(2)}(\zeta) = \frac{4(q-1)}{q}$. The nonclassical nature of the state is apparent, when one takes the value $q = 2$ where the function $g_a^{(2)}(\zeta) < 1$ as shown in Fig. 11(a). On the other hand when we take $q > 2$ the function $g_a^{(2)}(\zeta) > 2$ for higher values of ζ.

As soon as one takes the nonlinear functions $f_1(q-n)$ and $f_2(n)$ into consideration and adjusts the parameters $\eta = \eta_1 = \eta_1 = 0.3$ in Fig. 11(b) one can see that the starting points are unchanged for the three curves, but the interval of $|\zeta|$ for the full sub-Poissonian and super-Poissonian distributions are increasing. The super-thermal state behavior too is appearing, but the maximum values for the curves are decreased compared with the above case as observed in Fig. 11(b).

Further we consider the function $g_b^{(2)}(\zeta)$ for the second mode. In the case of $\eta = 0$ and q takes the values $3, 4$ and 5 we find that the function $g_b^{(2)}(\zeta)$ starts at 1.5, 1.33 and 1.25 respectively. Because of the condition between the two modes $(\hat{a}^\dagger\hat{a} + \hat{b}^\dagger\hat{b})$ is constant, thus when we take the limits as $\zeta \to 0$ we get the limit $g_b^{(2)}(\zeta) = \frac{q}{q-1}$. We see that $g_b^{(2)}(\zeta)$ has a decreasing trend and so for sufficiently large values of $|\zeta|$ it shows sub-Poissonian behavior because for $\zeta \to \infty$ we get the limit $g_b^{(2)}(\zeta) = \frac{q-1}{q}$. For further increase of q the state $|\zeta, q\rangle$ exhibits full sub-Poissonian behavior (see Fig. 11(c)). We note that the super-Poissonian distribution interval increases by increasing the parameter q. As it is exhibited by Figs. 11(a) and 11(c) the modes a and b behave differently for small values of $|\zeta|$ and also for large values of $|\zeta|$. However, both modes may show sub-Poissonian behavior. For example when we take $|\zeta| = \sqrt{2}$ and $q = 2$ it is found that $g_a^{(2)}(\zeta) = g_b^{(2)}(\zeta) = \frac{2}{3}$ which means sub-Poissonian behavior in both modes see [100, 101]. When we take the nonlinearity parameter $\eta = 0.3$ into account we find that when q is small there exists a short interval of $|\zeta|$ where the function $g_b^{(2)}(\zeta)$ reaches super-Poissonian state behavior, the distribution is lowered gradually to sub-Poissonian behavior as observed in Fig. 11(d).

4.3.2 Phase Properties

The quantum properties of the radiation field can be investigated under different points of view. Therefore we continue our progress and devote the present section to considering and discussing the phase distribution for the states (51). For this reason it is convenient to use the phase formalism introduced by Barnett and Pegg [88–95]. It is well known that the phase operator is defined as the projection operator on a particular phase state multiplied by the corresponding value of the phase. Therefore one can find that the Pegg-Barnett phases distribution function $P_{\zeta,q}(\theta_1, \theta_2)$ is given by [93–95]:

$$P_{\zeta,q}(\theta_1, \theta_2) = \frac{|N_q|^2}{(2\pi)^2} \sum_{n,m} \frac{\zeta^n f_1(q-n)!}{f_1(q)! f_2(n)!} \frac{\zeta^{*m} f_1(q-m)!}{(f_1(q)! f_2(m)!)^2} \sqrt{\frac{(q-n)!(q-m)!}{q!n!q!m!}}$$
$$\times \exp\big[i\big[(q-n)-(q-m)\big]\theta_1 + i(n-m)\theta_2\big]. \tag{73}$$

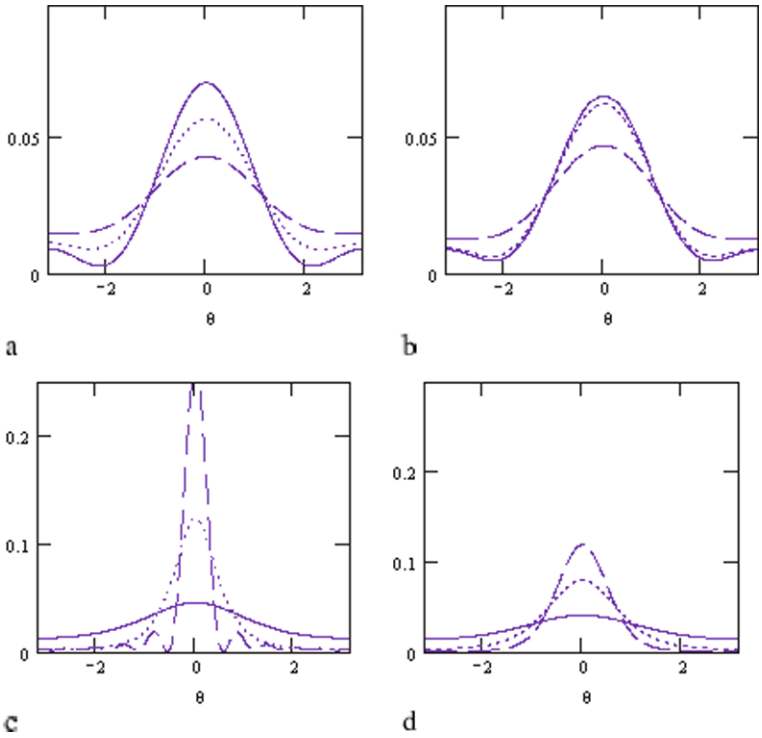

Fig. 12 The phase distribution $P_{\zeta,q}(\theta)$ against the angle $\theta = (\theta_2 - \theta_1)$, (**a**) $q = 1$ and $\eta = 0$, (**b**) $q = 10$ and $\eta = 0$, (**c**) $q = 1$ and $\eta = 0.3$, (**d**) $q = 10$ and $\eta = 0.3$, where the *solid curve* for $\zeta = 1$, the *dot curve* for $\zeta = 3$ and the *dash curve* for $\zeta = 5$

Therefore the phases distribution function can be written as

$$P_{\zeta,q}(\theta_1,\theta_2) = \frac{|N_q|^2}{(2\pi)^2}\left|\sum_n \frac{\zeta^n f_1(q-n)!}{f_1(q)!f_2(n)!}\sqrt{\frac{(q-n)!}{q!n!}}\exp[in\theta]\right|^2, \quad -\pi \le \theta \le \pi,\ \theta = \theta_2 - \theta_1. \tag{74}$$

Due to the correlation between the two modes, the phase distribution depends on the difference between the phases of the modes. In the figures we plot $P_{\zeta,q}(\theta)$ against the angle $\theta = \theta_2 - \theta_1$ for different valued of the parameter q, $|\zeta|$ and η.

The phase behavior for the present state we have plotted the function against the phase angle θ for $(\eta = 0)$ and different values of q same as above Sect. 2.3.2. As soon as one takes the nonlinear functions $f_1(q-n)$ and $f_2(n)$ into consideration and adjusts the parameters $\eta = 0.3$, we observe that a peak around $\theta = 0$ develops and increases by decreasing the parameter $|\zeta|$ as observed in Fig. 12(d). The behavior of the nonlinearity functions for the phase distribution in this case is the same as in the first case (small values of q).

5 Two Modes Parametric Converter

The problem of coupled oscillators are also playing an essential role in the nonlinear optical effects. These include Raman and Brillouin effects, Stokes and anti-Stokes generations,

etc. All these effects involve nonlinear coupling between various types of boson excitations such as phonons, spin waves, plasmons, protons, polaritons, etc., as well as electromagnetic waves. In the optical regime there are two of the most important nonlinear parametric interactions, they are frequency conversion and parametric amplification [131–143]. In the present section we shall generalize the usual JC model, however in a different direction. For this reason we shall consider two coupled fields in the form of frequency converter type (resultant of variation in the permeability) injected within a cavity where a 2-level atom passes, so we have an interaction between the coupled fields and the atom, as well as the field-field interaction. Therefore the system would acquire two different coupling parameters and the Hamiltonian describing such a system can be written as follows

$$\frac{\hat{H}}{\hbar}=\sum_{i=1}^{2}\omega_i\hat{a}_i^{\dagger}\hat{a}_i+\frac{\omega_0}{2}\sigma_z+i\lambda_1\big(\hat{a}_1^{\dagger}\hat{a}_2-\hat{a}_1\hat{a}_2^{\dagger}\big)(\sigma_+-\sigma_-)+\lambda_2\big(\hat{a}_1^{\dagger}\hat{a}_2+\hat{a}_1\hat{a}_2^{\dagger}\big), \tag{75}$$

where ω_i, $i=1,2$ is the ith mode frequency, and ω_0 is the frequency of two atomic energy levels difference, λ_1 is the coupling parameter that connects the field nonlinearly with the atom, while λ_2 is the coupling parameter responsible the field-field interaction. The operators $\hat{a}_i^{\dagger}$ and $\hat{a}_i$ are the fields creation and annihilation operators which satisfy the usual boson commutation relations. The operators $\sigma_+(\sigma_-)$, and σ_z are the usual raising (lowering) and inversion operators for the two-level atomic system.

The Hamiltonian model in this case can be regarded as a driven coupled oscillator within a cavity. Therefore it would be interesting to make a comparison between the present model and that of the atom-field interaction under action of an external electric field. Although both systems are different however, under an approximation one may manage to reduce the present model to the other one. To show that let us approximate one of the fields in (75) to its C-number, for example $\hat{a}_2\rightarrow|\alpha_2|\exp(-i\omega_2 t)$. In this case when we set $\hat{A}=\hat{a}_1\exp(i\omega_2 t)$, then the Hamiltonian (75) immediately transforms to the form

$$\frac{\hat{H}}{\hbar}=\widetilde{\omega}\hat{A}^{\dagger}\hat{A}+\frac{\omega_0}{2}\sigma_z+ig\big(\hat{A}^{\dagger}\sigma_--\hat{A}\sigma_+\big)+\bar{\lambda}_2\big(\hat{A}^{\dagger}+\hat{A}\big),\quad \widetilde{\omega}=(\omega_1-\omega_2), \tag{76}$$

which is exactly the driven JC model under action of a constant electric field. It should be noted that in the above equation we have applied the rotating wave approximation, and introduced new coupling parameters $g=\lambda_1|\alpha_2|$ and $\bar{\lambda}_2=\lambda_2|\alpha_2|$.

5.1 The Time Evolution Operator

As we have mentioned above our aim of the present work is to examine some properties of the system described by the Hamiltonian (75). Therefore we devote this section to find the tools to reach our goal. For this reason let us introduce the canonical transformation

$$\hat{a}_1=\hat{b}_1\cos\xi+\hat{b}_2\sin\xi,\qquad \hat{a}_2=\hat{b}_2\cos\xi-\hat{b}_1\sin\xi \tag{77}$$

where the operators $\hat{b}_i(\hat{b}_i^{\dagger})$, $i=1,2$ have the same meaning of the operators $\hat{a}_i(\hat{a}_i^{\dagger})$, $i=1,2$ while ξ is the rotation angle and will be determined later. It is easy to realize that the canonical transformation (77) always satisfy the conservation of total photon number law where

$$\hat{a}_1^{\dagger}\hat{a}_1+\hat{a}_2^{\dagger}\hat{a}_2=\hat{b}_1^{\dagger}\hat{b}_1+\hat{b}_2^{\dagger}\hat{b}_2. \tag{78}$$

Which means that the sum of the photon number is invariant under this transformation. Now if we insert (77) into (75), then after some calculations we have

$$\frac{\hat{H}}{\hbar} = \sum_{i=1}^{2} \overline{\omega}_i \hat{n}_i + \frac{\omega_0}{2}\hat{\sigma}_z + i\lambda_1\big(\hat{b}_1^{\dagger}\hat{b}_2\hat{\sigma}_+ - \hat{b}_2^{\dagger}\hat{b}_1\hat{\sigma}_-\big), \quad \hat{n}_i = \hat{b}_i^{\dagger}\hat{b}_i, \tag{79}$$

where the augmented frequencies are

$$\begin{aligned} \overline{\omega}_1 &= \omega_1 \cos^2\xi + \omega_2 \sin^2\xi - \lambda_2 \sin 2\xi, \\ \overline{\omega}_2 &= \omega_2 \cos^2\xi + \omega_1 \sin^2\xi + \lambda_2 \sin 2\xi, \\ \overline{\omega}_1 - \overline{\omega}_2 &= (\omega_1 - \omega_2)\cos 2\xi - 2\lambda_2 \sin 2\xi \end{aligned} \tag{80}$$

and

$$\xi = \frac{1}{2}\tan^{-1}\left(\frac{2\lambda_2}{\omega_1 - \omega_2}\right). \tag{81}$$

It should be noted that in the derivation of the above Hamiltonian we have applied the rotating wave approximation (RWA) with respect to the rotated operators $\hat{b}_i$ and $\hat{b}_i^{\dagger}$, not to the original (physical) operators $\hat{a}_i$ and $\hat{a}_i^{\dagger}$. Now we look for the evolution operator from which we will be able to obtain the dynamical operators for the present system. To do so let us first write the equation of the motion in the Heisenberg picture thus

$$\frac{d\hat{n}_1}{dt} = -\frac{d\hat{n}_2}{dt} = \frac{1}{2}\frac{d\hat{\sigma}_z}{dt} = \lambda_1\big(\hat{b}_1^{\dagger}\hat{b}_2\hat{\sigma}_+ + \hat{b}_1\hat{b}_2^{\dagger}\hat{\sigma}_-\big), \tag{82}$$

from which we can define the constants of the motion

$$\hat{N}_1 = \hat{n}_1 - \frac{1}{2}\hat{\sigma}_z, \qquad \hat{N}_2 = \hat{n}_2 + \frac{1}{2}\hat{\sigma}_z. \tag{83}$$

Using (83) together with (79) then the Hamiltonian model can be cast in the form

$$\frac{\hat{H}}{\hbar} = \hat{C} + \hat{N}, \tag{84}$$

$\hat{C}$ and $\hat{N}$ are constants of the motion given by

$$\hat{C} = \frac{\Delta}{2}\hat{\sigma}_z + i\lambda_1\big(\hat{b}_1^{\dagger}\hat{b}_2\hat{\sigma}_+ - \hat{b}_2^{\dagger}\hat{b}_1\hat{\sigma}_-\big), \qquad \hat{N} = \sum_{i=1}^{2}\overline{\omega}_i\hat{N}_i, \tag{85}$$

and $\Delta = (\overline{\omega}_1 - \overline{\omega}_2 + \omega_0)$ is the detuning parameter and it can be written as $\Delta = \delta - 2(\omega_1 - \omega_2)\sin^2\xi - 2\lambda_2 \sin 2\xi$ with $\delta = \omega_0 - (\omega_2 - \omega_1)$. Note that the detuning parameter Δ depends on the field-field couples parameter λ_2. Since the constant operators $\hat{C}$ and $\hat{N}$ commute then the evolution operator $\hat{U}(t)$ can be written as

$$\hat{U}(t) = \exp(-i\hat{H}t/\hbar) = \exp(-i\hat{N}t)\exp(-i\hat{C}t), \tag{86}$$

where

$$\exp(-i\hat{N}t) = \begin{bmatrix} \exp(-i\hat{W}_1 t) & 0 \\ 0 & \exp(-i\hat{W}_2 t) \end{bmatrix} \tag{87}$$

with

$$\hat{W}_1(\hat{n}_1,\hat{n}_2)=\overline{\omega}_1\left(\hat{n}_1-\frac{1}{2}\right)+\overline{\omega}_2\left(\hat{n}_2+\frac{1}{2}\right),\qquad \hat{W}_2(\hat{n}_1,\hat{n}_2)=\hat{W}_1(\hat{n}_1+1,\hat{n}_2-1),\quad (88)$$

and

$$\exp(-i\hat{C}t)=\begin{bmatrix}(\cos\hat{\mu}_1t-\frac{i\Delta}{2\hat{\mu}_1}\sin\hat{\mu}_1t) & \lambda_1\hat{b}_1^{\dagger}\hat{b}_2\frac{\sin\hat{\mu}_1t}{\hat{\mu}_1}\\ -\lambda_1\frac{\sin\hat{\mu}_1t}{\hat{\mu}_1}\hat{b}_1\hat{b}_2^{\dagger} & (\cos\hat{\mu}_2t+\frac{i\Delta}{2\hat{\mu}_2}\sin\hat{\mu}_2t)\end{bmatrix},\quad (89)$$

where we have used the abbreviations

$$\hat{\mu}_j^2(\hat{n}_1,\hat{n}_2)=\frac{\Delta^2}{4}+\hat{\nu}_j(\hat{n}_1,\hat{n}_2),\quad j=1,2,\quad (90)$$

$$\hat{\nu}_1(\hat{n}_1,\hat{n}_2)=\lambda_1^2\hat{n}_1(\hat{n}_2+1),\qquad \hat{\nu}_2(\hat{n}_1,\hat{n}_2)=\hat{\nu}_j(\hat{n}_1+1,\hat{n}_2-1).\quad (91)$$

After we introduce an appropriate state for the above system we shall employ the results obtained here to discuss the atomic inversion as well as the entropy squeezing. This will be seen in the forthcoming sections.

5.2 Correlated Converter States and Density Matrix

Before we discuss the behavior of the atomic inversion through the collapse and revival phenomenon, let us first derive the density matrix operator $\hat{\rho}(t)$ which we shall use to calculate the atomic inversion. For this reason we consider at time $t=0$ that the two-level atom is in a coherent superposition state of the excited state $|e\rangle$ and ground state $|g\rangle$, such that

$$|\theta,\phi\rangle=\cos\theta|e\rangle+e^{-i\phi}\sin\theta|g\rangle,\quad (92)$$

where ϕ is the relative phase of the two atomic levels and θ is the atomic coherence angle. Here we may point out that when we take $\theta\to 0$ then the excited state can be found, while for $\theta\to\pi/2$, then the wave function describes the atom in the ground state.

Now if we assume that at time $t=0$ the system is in a pure state, such that the wave function $|\psi(0)\rangle=|\theta,\phi\rangle\otimes|\xi,q\rangle$, then for $t>0$, the wave function takes the form

$$\begin{aligned}\big|\psi(t)\big\rangle&=\exp\{-i\hat{W}_1t\}\left\{\left(\cos\hat{\mu}_1t-\frac{i\Delta}{2\mu_1}\sin\hat{\mu}_1t\right)\cos\frac{\theta}{2}+\lambda_1\hat{b}_1^{\dagger}\hat{b}_2\frac{\sin\hat{\mu}_1t}{\hat{\mu}_1}\right.\\&\quad\left.\times\exp\{-i\phi\}\sin\frac{\theta}{2}\right\}|\xi,q,e\rangle+\exp\{-i\hat{W}_2t\}\left\{\left(\cos\hat{\mu}_2t+\frac{i\Delta}{2\mu_2}\sin\hat{\mu}_2t\right)\right.\\&\quad\left.\times\exp\{-i\phi\}\sin\frac{\theta}{2}-\lambda_1\frac{\sin\hat{\mu}_1t}{\hat{\mu}_1}\hat{b}_1\hat{b}_2^{\dagger}\cos\frac{\theta}{2}\right\}|\xi,q,g\rangle\\&=\big|D(t),e\big\rangle+\big|T(t),g\big\rangle.\end{aligned}\quad (93)$$

Where the states $|D(t)\rangle$ and $|T(t)\rangle$ are given by

$$\begin{aligned}\big|D(t)\big\rangle&=\exp\big\{-i\hat{W}_1(\hat{n}_1,\hat{n}_2)t\big\}\left\{\left(\cos\hat{\mu}_1(\hat{n}_1,\hat{n}_2)t-\frac{i\Delta}{2\mu_1(\hat{n}_1,\hat{n}_2)}\sin\hat{\mu}_1(\hat{n}_1,\hat{n}_2)t\right)\cos\frac{\theta}{2}\right.\\&\quad\left.+\lambda_1\hat{b}_1^{\dagger}\hat{b}_2\frac{\sin\hat{\mu}_1(\hat{n}_1,\hat{n}_2)t}{\hat{\mu}_1(\hat{n}_1,\hat{n}_2)}\exp\{-i\phi\}\sin\frac{\theta}{2}\right\}|\xi,q\rangle,\end{aligned}\quad (94)$$

and

$$|T(t)\rangle = \exp\{-i\hat{W}_2(\hat{n}_1,\hat{n}_2)t\}\Bigg\{\Bigg(\cos\hat{\mu}_2(\hat{n}_1,\hat{n}_2)t + \frac{i\Delta}{2\mu_2(\hat{n}_1,\hat{n}_2)}\sin\hat{\mu}_2(\hat{n}_1,\hat{n}_2)t\Bigg)\exp\{-i\phi\}\sin\frac{\theta}{2} - \lambda_1\frac{\sin\hat{\mu}_1(\hat{n}_1,\hat{n}_2)t}{\hat{\mu}_1(\hat{n}_1,\hat{n}_2)}\hat{b}_1\hat{b}_2^{\dagger}\cos\frac{\theta}{2}\Bigg\}|\xi,q\rangle. \tag{95}$$

The time-dependent analytical solution for the density operator of final state of the system may be written as follows

$$\hat{\rho}(t) = |D(t),e\rangle\langle e,D(t)| + |T(t),g\rangle\langle e,D(t)| + |D(t),e\rangle\langle g,T(t)| + |T(t),g\rangle\langle g,T(t)|. \tag{96}$$

In what follows we employ the density matrix operator given above to investigate some statistical properties of the field related to the present system, for example the atomic inversion. This will be seen in the next section.

5.3 Atomic Inversion

As we have mentioned above the atomic inversion represents non-trivial physical quantity which is defined as the difference between the probabilities of finding the atom in the exited state and in the ground state. In fact discussion of the atomic inversion gives us a light on the behavior of the atom-field interaction through the collapse and revival phenomenon. The atomic inversion $W(t)$ can be written as

$$W(t) = \frac{1}{2}\{\langle D(t)|D(t)\rangle - \langle T(t)|T(t)\rangle\}. \tag{97}$$

Using (94), and (95) together with (97) we have managed to plot Fig. 14 to discuss the collapses and revival phenomenon related to the present system. For example we have plotted the atomic inversion against the scaled time $\lambda_1 t$ for different values of the coupling parameter λ_2 and the detuning parameter Δ, keeping in mind that the atom is initially in the excited state ($\theta = 0$) and the field prepared to be in the correlated converter (finite dimensional PCS) state with variable parameters q and ξ and fixed frequencies at $\omega_1 = 0.8\lambda_1$ and $\omega_2 = 0.3\lambda_1$.

At exact resonance ($\delta = 0$) with $q = 10$ and $\xi = 3$ while λ_2 is zero, the function shows irregular rapid fluctuations around zero (as should be expected) with its extrema between $\sim \pm 0.4$ see Fig. 13(a). In the fluctuations of the atomic inversion in this case can be compared with the case of a weak thermal field [144]. This is expected because when we plot the photon distribution probability $P(n, q-n)$ for the parameters $\xi = 3, q = 10$ it almost resembles that case of a thermal field with $\bar{n}_1 = 1.02$ see Fig. 14(f). When the second field coupling parameter is involved ($\frac{\lambda_2}{\lambda_1} = 0.9$) the general behavior of the function is not unchanged markedly however it shows a slight decreasing in its amplitude. Moreover we can observe that the fluctuations in this case have a slight interference between patterns compared with the previous case. This may due to the presence of the coupling parameter λ_2 which increases the energy exchange between the fields, see Fig. 13(b). Introducing the field-field coupling results in adding detuning in the system, since from (80), (81), (85) we can write the detuning parameter in the form $\Delta = \delta + (\omega_2 - \omega_1) - \frac{(\omega_2-\omega_1)^2 - 4\lambda_2^2}{\sqrt{(\omega_2-\omega_1)^2+4\lambda_2^2}}$. This shows

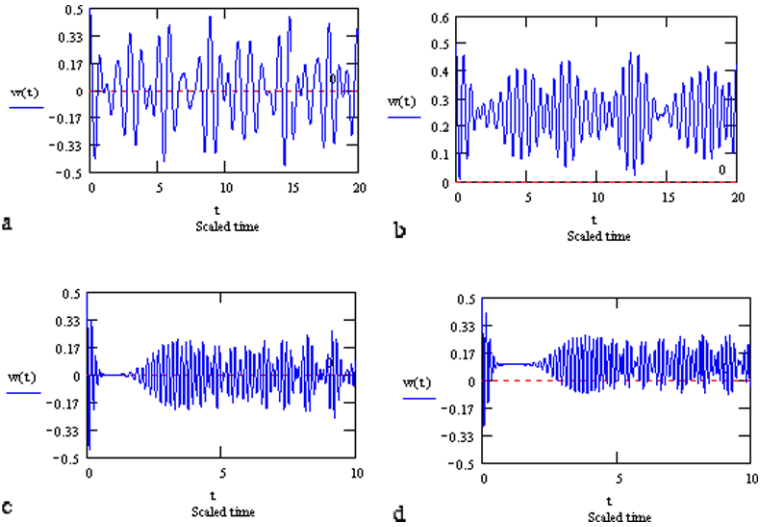

Fig. 13 The time evolution of the atomic inversion as a function of the scaled time $\lambda_1 t$, with the atom initially in excited state ($\theta = 0$) and the field is prepared in correlated converter state with fixed parameters $\omega_1/\lambda_1 = 0.8$, and $\omega_2/\lambda_1 = 0.3$ (**a**) $\xi = 3$, $q = 10$, $\lambda_2 = 0$, $\delta = 0$, (**b**) $\xi = 3$, $q = 10$, $\lambda_2 = 0.9\lambda_1$, $\delta = 0$, (**c**) $\xi = 3$, $q = 10$, $\lambda_2 = 0.9\lambda_1$, $\delta = 5\lambda_1$, (**d**) $\xi = 18$, $q = 50$, $\lambda_2 = 0.9\lambda_1$, $\delta = 20\lambda_1$

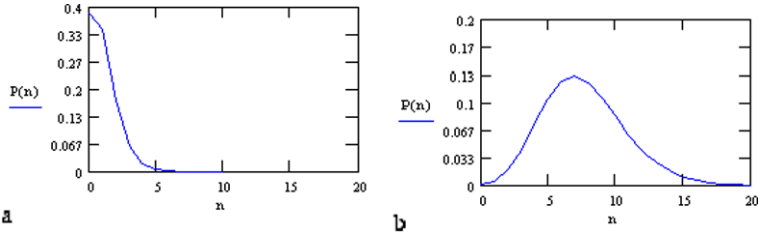

Fig. 14 The photon distribution probability $P(n, q-n)$ for the parameters (**a**) $\xi = 3$, $q = 10$, (**b**) $\xi = 18$, $q = 50$

clearly the dependence of the detuning on the coupling λ_2 and increasing its value results in increasing the detuning, which in turn lowers the amplitude of the fluctuations and increases its oscillations. Therefore we can adjust the different parameters to get any designed Δ.

As soon as the detuning parameter is increased further ($\delta = 5\lambda_1$) the atomic inversion shifts its value upward to fluctuate around 0.25, but with more interference between patterns and fast oscillations. However, the general shape of the function is not changed markedly see Fig. 14(c). Another interesting phenomenon can be observed when we increase the value of both ($q = 50$) and ($\xi = 18$) even in absence of the detuning parameter Δ. The plot for the photon probability distribution $P(n) = |\langle n, q-n|\xi, q\rangle|^2$ resembles an almost Poissonian distribution with $\bar{n}_2 = 7.7$ see Fig. 14(g). Hence the appearance of the collapse and the first revival. However, the term of revival here can not be given by the formula for the standard JCM (see [145]). As time develops another phenomenon starts to be exhibited. This phenomenon is known as *a superstructure phenomenon* where we can see more building up of irregular fluctuations with a strong interference between patterns. This means that if the number of photons are increased in a correlated manner then the *superstructure phenomenon*

may be observed. Moreover the collapse period in this case is too short and occurs nearly after one set of the interaction. Also the function fluctuates around zero (as usual) where $\Delta = 0$ and its amplitude reaches the extrema after considerable period of time see Fig. 13(c). Finally when we have taken the second field coupling parameter λ_2 into consideration as well as the detuning parameter ($\Delta = 17.9$) see Fig. 13(d), the function is shifted upward and fluctuates around ~ 0.1 showing negative values on contrary to the case in which $q = 10$ and $\xi = 3$ where the atomic inversion never reaches zero value at any period of time in Fig. 13(d). The correlated converter finite dimensional PCS state this shows different behavior from the behavior of the standard JCM in both cases of thermal or coherent fields. This is due to the structure of this correlated state.

5.4 Entropy and Variances Squeezing

The argument for using entropic uncertainty relations for two-level system rather than the Heisenberg uncertainty relations to investigate quantum fluctuations was recently discussed in [146–151]. In quantum mechanical system with two physical observables represented by the Hermitian operators $\hat{A}$ and $\hat{B}$ satisfying the commutation relation $[\hat{A}, \hat{B}] = i\hat{C}$, one can write the Heisenberg uncertainty relation in the form

$$\left\langle (\Delta\hat{A})^2 \right\rangle \left\langle (\Delta\hat{B})^2 \right\rangle \geq \frac{1}{4}\left|\langle \hat{C} \rangle\right|^2, \tag{98}$$

where $\langle (\Delta\hat{A})^2 \rangle = (\langle \hat{A}^2 \rangle - \langle \hat{A} \rangle^2)$. Consequently, the uncertainty relation for a two-level atom characterized by the Pauli operators $\hat{\sigma}_x$, $\hat{\sigma}_y$ and $\hat{\sigma}_z$, satisfying the commutation $[\hat{\sigma}_x, \hat{\sigma}_y] = i\,\hat{\sigma}_z$ can also be written as $\Delta\hat{\sigma}_x \Delta\hat{\sigma}_y \geq \frac{1}{2}|\langle \hat{\sigma}_z \rangle|$.

Fluctuations in the component $\hat{\sigma}_\alpha$ of the atomic dipole is said to be squeezed if $\hat{\sigma}_\alpha$ satisfies the condition

$$V(\hat{\sigma}_\alpha) = \left(\Delta\hat{\sigma}_\alpha - \sqrt{\left| \frac{\langle \hat{\sigma}_z \rangle}{2} \right|} \right) < 0, \quad \alpha = x \text{ or } y. \tag{99}$$

In an even N-dimensional Hilbert space, the investigation of the optimal entropic uncertainty relation for sets of $N + 1$ complementary observables with the non-degenerate eigenvalues can be described by the inequality [148–151]

$$\sum_{k=1}^{N+1} H(\hat{\sigma}_k) \geq \frac{N}{2} \ln\left(\frac{N}{2}\right) + \left(1 + \frac{N}{2}\right) \ln\left(1 + \frac{N}{2}\right), \tag{100}$$

where $H(\hat{\sigma}_k)$ represents the information entropy of the variable $\hat{\sigma}_k$. On the other hand, for an arbitrary quantum state the probability distribution for N possible outcomes of measurements of the operator $\hat{\sigma}_\alpha$ is $P_i(\hat{\sigma}_\alpha) = \langle \Psi_{\alpha i} | \rho | \Psi_{\alpha i} \rangle$, where $|\Psi_{\alpha i}\rangle$ is an eigenvector of the operator $\hat{\sigma}_\alpha$ such that $\hat{\sigma}_\alpha |\Psi_{\alpha i}\rangle = \lambda_{\alpha i} |\Psi_{\alpha i}\rangle$, $\alpha = x, y, z$, $i = 1, 2, \ldots, N$. The corresponding Shannon information entropies are then defined as

$$H(\hat{\sigma}_\alpha) = -\sum_{i=1}^{N} P_i(\hat{\sigma}_\alpha) \ln P_i(\hat{\sigma}_\alpha), \quad \alpha = x, y, z. \tag{101}$$

To obtain the Shannon information entropies of the atomic operators $\hat{\sigma}_x$, $\hat{\sigma}_y$ and $\hat{\sigma}_z$ for a two-level atom, with $N = 2$, one can use the reduced atomic density operator $\hat{\rho}(t)$. Thus we

have the following expression,

$$H(\hat{\sigma}_\alpha) = -\frac{1}{2}\big[\rho_\alpha(t)+1\big]\ln\bigg[\frac{1}{2}\big[\rho_\alpha(t)+1\big]\bigg] - \frac{1}{2}\big[1-\rho_\alpha(t)\big]\ln\bigg[\frac{1}{2}\big[1-\rho_\alpha(t)\big]\bigg], \quad \alpha = x, y, z. \tag{102}$$

Since the uncertainty relation of the entropy can be used as a general criterion for the squeezing of an atom, therefore for a two-level atom where $N = 2$, we have $0 \leq H(\hat{\sigma}_\alpha) \leq \ln 2$, and hence from (102), the Shannon information entropies of the operators $\hat{\sigma}_x$, $\hat{\sigma}_y$, $\hat{\sigma}_z$ will satisfy the inequality

$$H(\hat{\sigma}_x) + H(\hat{\sigma}_y) + H(\hat{\sigma}_z) \geq 2\ln 2. \tag{103}$$

In other words if we define $\delta H(\hat{\sigma}_\alpha) = \exp[H(\hat{\sigma}_\alpha)]$, then we can write

$$\delta H(\hat{\sigma}_x)\delta H(\hat{\sigma}_y)\delta H(\hat{\sigma}_z) \geq 4. \tag{104}$$

It is interesting to mention that the above inequality, was previously obtained and established to be optimal. The fluctuations in component $\hat{\sigma}_\alpha$ ($\alpha = x$ or y) of the atomic dipole are said to be "squeezed in entropy" if the Shannon information entropy $H(\hat{\sigma}_\alpha)$ of $\hat{\sigma}_\alpha$ satisfies the condition,

$$E(\hat{\sigma}_\alpha) = \delta H(\hat{\sigma}_\alpha) - \frac{2}{\sqrt{\delta H(\hat{\sigma}_z)}} < 0, \tag{105}$$

where $\alpha = x$ or y.

The time dependent density matrix is given by $\rho_\alpha(t) = \langle\psi(0)|\rho_\alpha(t)|\psi(0)\rangle$, then after some manipulations we can get the expression of the density matrix in the form

$$\begin{aligned} &\rho_x(t) = 2Re\big[\big\langle\big|D(t)\big|T(t)\big\rangle\big], \qquad \rho_y(t) = 2Im\big[\big\langle\big|D(t)\big|T(t)\big\rangle\big], \\ &\rho_z(t) = \big\langle D(t)\big|D(t)\big\rangle - \big\langle T(t)\big|T(t)\big\rangle, \end{aligned} \tag{106}$$

where $|D(t)\rangle$, $|T(t)\rangle$ defined by (94), (95) respectively.

In what follows we examine the temporal evolutions of the entropy squeezing as well as variances squeezing related to the present system. We present several figures of the entropy squeezing $E(\hat{\sigma}_x)$ and $E(\hat{\sigma}_y)$, and the variance squeezing factors $V(\hat{\sigma}_x)$ and $V(\hat{\sigma}_y)$, against the scaled time $\lambda_1 t$ for an initially excited atom ($\theta = 0$). Furthermore we have considered the field initially in correlated converter state with fixed values of the field frequencies ($\omega_1 = 0.8\lambda_1$ and $\omega_2 = 0.3\lambda_1$), however with various values of the other parameters.

For example, in Fig. 15 we have considered $q = 10$ and $\xi = 3$, and examined the system at exact resonance such that $\delta = 0$ and $\lambda_2 = 0$. In this case we observe squeezing occurring several times in the first quadrature $E(\hat{\sigma}_x)$ where its maximum (minimum value of the function) occurs approximately periodic in the considered interval of time. In the meantime this phenomenon is absent from the second quadrature $E(\hat{\sigma}_y)$, however we realize that the maximum value of the entropy squeezing is fixed just above 0.05. On the other hand we see squeezing strongly occurring several times in variance squeezing quadrature $V(\hat{\sigma}_x)$ with period longer than that of the entropy squeezing quadratures. This phenomenon is absent from the second variance squeezing quadrature $V(\hat{\sigma}_y)$. Also we may refer to the irregular fluctuations in all quadratures and the patterns interference which is less pronounced in the

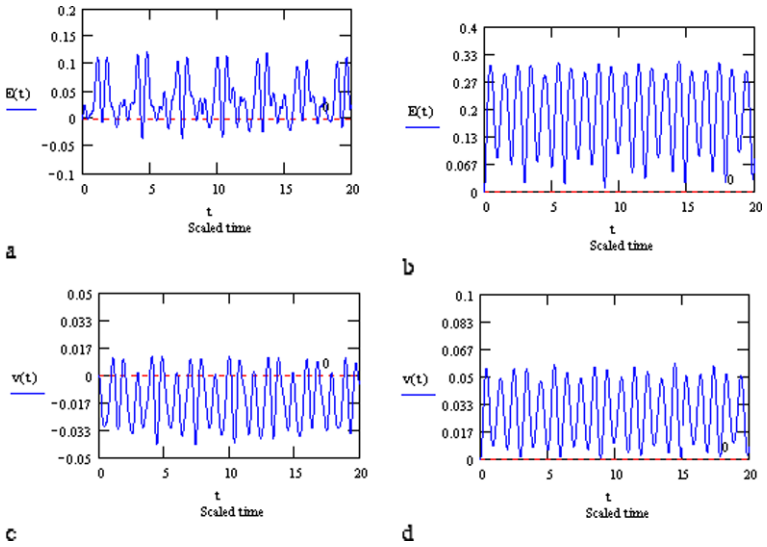

Fig. 15 The time evolution of the entropy squeezing and the variance squeezing as a function of the scaled time $\lambda_1 t$, with the atom initially in excited state ($\theta = 0$) and the field is prepared in correlated converter state with fixed parameters $\omega_1/\lambda_1 = 0.8$, and $\omega_2/\lambda_1 = 0.3$ and with parameters $\lambda_2 = 0$, $\delta = 0$, $q = 10$, and $\xi = 3$ where (**a**) the entropy squeezing factor $E(\hat{\sigma}_x)$; (**b**) the entropy squeezing factor $E(\hat{\sigma}_y)$; (**c**) the variance squeezing factor $V(\hat{\sigma}_x)$; (**d**) the variance squeezing factor $V(\hat{\sigma}_y)$

variance squeezing factors $V(\hat{\sigma}_{x,y})$ than for the entropy squeezing $E(\hat{\sigma}_{x,y})$. We must note here that for the coherent input [148–152] or two-mode nonlinear coherent states [153–155].

As soon as one takes the coupling parameter λ_2 into consideration and adjusts the detuning parameter $\Delta = 3$ (Fig. 16) one can see that the entropy squeezing reduced its amount in the first quadrature $E(\hat{\sigma}_x)$ compared with the previous case, while there is squeezing in the quadrature $E(\hat{\sigma}_y)$ at some points. The variance squeezing factors in this case also acquire squeezing, however with amounts less than the previous case. We note that for the variance squeezing, the squeezing in $V(\hat{\sigma}_x)$ and the squeezing in $V(\hat{\sigma}_y)$ alternate periodically in Figs. 16(c) and 16(d). Clearly in this case the picture is even more distinct than the previous investigations [146–155]. The investigation so far has considered the case of the state $|10, 3\rangle$ which involved few photon state as $P(n)$ shows.

When we increase the value of the parameters $q = 50$ and $\xi = 18$ corresponding to increasing the mean photon numbers and the detuning parameter Δ to 17.8 as in Fig. 17 a marked change occurs in both entropy squeezing and variance squeezing factors $E(\hat{\sigma}_{x,y})$ and $V(\hat{\sigma}_{x,y})$. This can be seen in Fig. 17 where the squeezing is observed in $E(\hat{\sigma}_x)$ and not in $E(\hat{\sigma}_y)$. Also the atomic system loses some of its energy to the system the squeezing of all quantities starts in the entropies, but for the variances no squeezing appeared as observed in Fig. 17. However the entropy squeezing and variance squeezing display fluctuations with interference of patterns which reflects the effect of the Poissonian distribution as Fig. 17(b) shows.

6 Conclusion

In this review we have discussed and proposed a scheme for generating a correlated two-mode finite dimensional states in the vibrational motion of a trapped ion in two dimensional

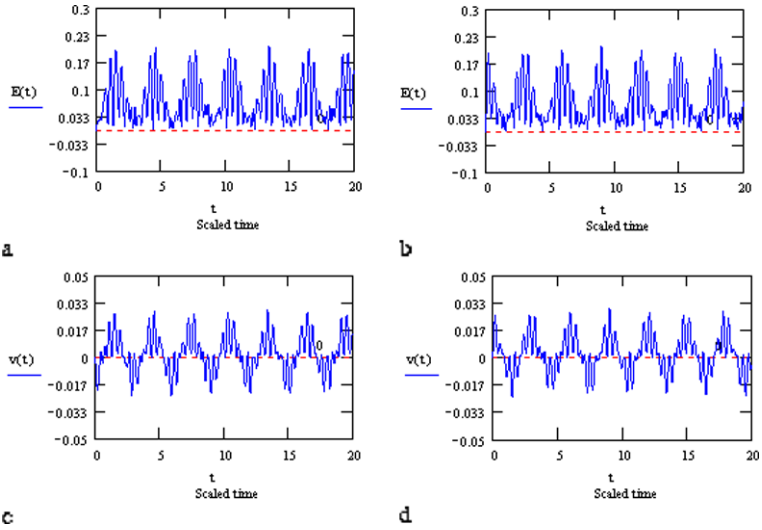

Fig. 16 As Fig. 15 but with $\delta = 5\lambda_1$

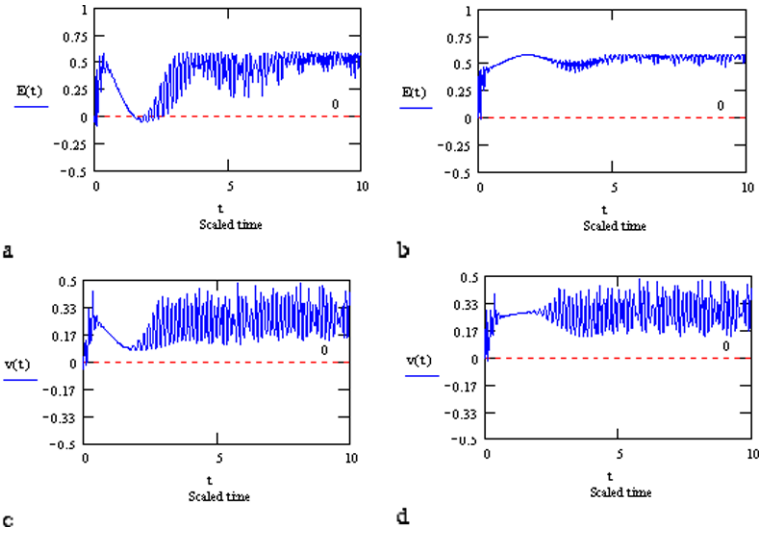

Fig. 17 As Fig. 15 but with $q = 50$, and $\xi = 18$ and $\delta = 20\lambda_1$

harmonic potential. These states generated by this scheme are stable because they appear in a steady regime in which the ion has fully relaxed to its ground state. If the vibrational state of motion of the ion is initially prepared in this state, then the steady state of the system is a pure state given by a product of the atomic ground state with a state (4) of the vibrational motion. In this case, the two parameters, ζ and q that characterize the two-mode finite dimensional states are determined by the intensities and phases of the driving lasers, the Lamb-Dicke parameter and by the sum of the phonon number of the two vibrational modes. Based on recent technology techniques the present scheme could be realized experimentally

[80, 81]. Quantum statistical properties of these states have been studied in detail. We have found interesting nonclassical features of these states. The sub-Poissonian distribution and the phase distribution were displayed for particular values of the parameters.

We have introduced new class of nonclassical states, which are referred as superposition of finite dimensional pair coherent states. Mathematically, these states are simultaneous eigenstates of the operator $(\hat{a}^{\dagger}\hat{b} + \frac{\zeta^{q+1}(\hat{a}\hat{b}^{\dagger})^{q}}{(q!)^{2}})^{2}$ and the operators that give the relative occupation numbers of the two modes. Physically, these states can be produced by processes in which there is a strong competition between a two mode parametric conversion. We have considered some statistical properties of these states. For example, we have considered the Glauber second-order correlation function $g^{(2)}(|\zeta|)$, which shows that the state at $j = 0$ is partially nonclassical for large values of the parameter q with respect to the first mode but for the second is fully nonclassical for a short range of $|\zeta|$ for any values of q. The violation of Cauchy-Schwarz inequalities has been studied in detail. We found the violation depends sensitively on j $(j = 0, 1)$, and the parameter q. The phase properties distribution in the Pegg-Barnett approach applied to such states showed that it has a central peak and two wings. We have obtained the formulae for the s-parameterized CF for such state. The interference behavior in phase space for the Wigner function has been shown. Nonclassical signatures for the states have been observed from negativity of Wigner function. Finally the Q-function for some parameters is presented analytically and numerically. We found that both of them are greatly effected with any variation in the parameter q and the parameter ζ.

Also in this work, we have studied an extension to a nonlinear finite-dimensional pair coherent state and proposed a scheme for generating in the vibrational motion of a trapped ion in two-dimensional harmonic potential. These states generated by this scheme are stable because they appear in a steady regime in which the ion has fully relaxed to its ground state. If the vibrational state of motion of the ion is initially formed in this state, then the steady state of the system is a pure state given by a product of the atomic ground state with form (51) of the vibrational motion. In this case, the three parameters, ζ, q and η, that characterize the two-mode nonlinear finite-dimensional states are determined by the intensities and phases of the driving lasers, the Lamb-Dicke parameter and by the sum of the phonon number of the two vibrational modes. The effect of the nonlinearity function is shown for the sub-Poissonian and phase distributions. The behavior of the sub-Poissonian distribution function depends on the values of nonlinearity function and q parameter. Comparisons between the nonlinear finite-dimensional pair coherent state and the standard finite-dimensional pair coherent state have been made for the different phenomena. These states may find applications in the fields of quantum optics and quantum information.

We studied the finite dimensional state as the initial state for the system of a Hamiltonian model that consists of two types of the interaction. The first kind is linear and represents field-field interaction (frequency conversion), while the second kind is non-linear and represents atom-field interaction. Exact solution of the wave function is obtained. Also use the density matrix from which we have managed to discuss the behavior of the atomic inversion through the revival and collapses phenomena. The behavior of entropy squeezing and variance squeezing factors are also considered. We found that both of them are drastically effected with any variation in the detuning parameter and the second field coupling parameter, as well as the mean photon numbers. The state of the field has its fingerprints clearly on the shape of the squeezing parameters and differentiates it from other states as has been discussed above.

Acknowledgements The authors wish to thank the referees for their valuable comments that resulted in improvements of the paper in many aspects.

References

1. Kim, Y.S., Man'ko, M.A., Sergienko, A. (eds.): J. Opt. B: Quantum Semiclass. Opt. **4**, S91 (2002), one special issue on Uncertainty relations, quantum phase space, quantum optics, quantum information, imaging and computing
2. Zanardi, P.: Phys. Rev. A **65**, 042101 (2002)
3. Jennewein, T., Simon, C., Weihs, G., Weinfurter, H., Zeilinger, A.: Phys. Rev. Lett. **84**, 4729 (2000)
4. Furusawa, A., Sorensen, J., Braunstein, S.L., Fuchs, C.A., Kimble, H.J., Polzik, E.S.: Science **282**, 706 (1998)
5. Grover, L.K.: Phys. Rev. Lett. **79**, 325 (1997)
6. Wu, X.H., Xie, R.H., Huang, X.D., Hsia, Y.F.: Phys. Rev. A **53**, R1927 (1996)
7. Bennett, C.H.: Phys. Rev. Lett. **69**, 2881 (1992)
8. Kok, P., Munro, W.J., Nemoto, K., Ralph, T.C., Dowling, J.P., Milburn, G.J.: Rev. Mod. Phys. **79**, 135 (2007)
9. Bouwmeester, D., Eckert, A., Zeilinger, A. (eds.): The Physics of Quantum Information. Springer, Berlin (2000)
10. Peters, N.A., Altepeter, J.B., Branning, D., Jeffrey, E.R., Wei, T.-C., Kwiat, P.G.: Phys. Rev. Lett. **92**, 133601 (2004)
11. Garbaczewski, P.: Appl. Math. Inform. Sci. **1**, 1 (2007)
12. Jacquod, Ph.: Phys. Rev. Lett. **92**, 150403 (2004)
13. Abdel-Aty, M.: Laser Phys. Lett. **2**, 104 (2004)
14. De Martinil, F., Sciarrino, F.: J. Phys. A: Math. Theory **40**, 2977 (2007)
15. Ficek, Z.: Appl. Math. Inform. Sci. **3**, 375 (2009)
16. Horodecki, R., Horodecki, M., Horodecki, P.: Phys. Rev. A **59**, 1799 (1999)
17. Josse, V., Dantan, A., Bramati, A., Pinard, M., Giacobino, E.: Phys. Rev. Lett. **92**, 123601 (2004)
18. van Loock, P., Braunstein, S.L.: Phys. Rev. Lett. **84**, 3482 (2000)
19. Nguyen, B.A.: Phys. Rev. A **68**, 022321 (2003)
20. van Loock, P., Braunstein, S.L.: Phys. Rev. Lett. **87**, 247901 (2001)
21. Fu, H., Feng, Y., Solomon, A.I.: J. Phys. A **33**, 2231 (2000)
22. Barranco, A.V., Roversi, J.: Phys. Rev. A **50**, 5233 (1994)
23. Dodonov, V.V.: J. Opt. B: Quantum Semiclass. Opt. **4**, R1 (2002)
24. Klauder, J.R., Skagerstam, B.-S.: Coherent States. Applications in Physics and Mathematical Physics. World Scientific, Singapore (1985)
25. Perelomov, A.: Generalized Coherent States and Their Applications. Springer, Berlin (1986)
26. Klauder, J.R.: J. Math. Phys. **4**, 1055 (1963)
27. Nieto, M.H., Simmons, L.M.: Phys. Rev. Lett. **41**, 207 (1978)
28. Biedenharn, L.C.: J. Phys. A: Math. Gen. **22**, L873 (1989)
29. Macfarlane, A.J.: J. Phys. A: Math. Gen. **22**, 4581 (1989)
30. de Matos Filho, R.L., Vogel, W.: Phys. Rev. A **54**, 4560 (1996)
31. Manko, V.I., Marmo, G., Sudarshan, E.C.G., Zaccaria, F.: Phys. Scr. **55**, 528 (1997)
32. Agarwal, G.S.: J. Opt. Soc. Am. B **5**, 1940 (1988)
33. Agarwal, G.S.: Phys. Rev. Lett. **57**, 827 (1986)
34. Khalil, E.M., Abd Al-Kader, G.M.: Appl. Math. Inform. Sci. **1**, 35 (2007)
35. Saif, F., Abdel-Aty, M., Javed, M., Ul-Islam, R.: Appl. Math. Inform. Sci. **1**, 323 (2007)
36. Gou, S.-C., Steinbach, J., Knight, P.L.: Phys. Rev. A **54**, 4315 (1996)
37. Diedrich, F., Bergquist, J.C., Itano, W.M., Wineland, D.J.: Phys. Rev. Lett. **62**, 403 (1989)
38. Monroe, C., Meekhof, D.M., King, B.E., Jefferts, S.R., Itano, W.M., Wineland, D.J.: Phys. Rev. Lett. **75**, 4011 (1995)
39. Blockley, C.A., Walls, D.F., Risken, H.: Eur. Lett. **17**, 509 (1992)
40. Cirac, J.I., Blatt, R., Parkins, A.S., Zoller, P.: Phys. Rev. Lett. **70**, 762 (1993)
41. Cirac, J.I., Blatt, R., Zoller, P.: Phys. Rev. A **49**, R3174 (1994)
42. Cirac, J.I., Parkins, A.S., Blatt, R., Zoller, P.: Phys. Rev. Lett. **70**, 556 (1993)
43. Jaynes, E.T., Cummings, F.W.: Proc. IEE **51**, 89 (1963)
44. See references in the review article Shore, B.W., Knight, P.L.: J. Mod. Opt. **40**, 1195 (1993)
45. Abdalla, M.S., Ahmed, M.M.A., Obada, A.-S.F.: Physica A **162**, 215 (1990)
46. Abdalla, M.S., Ahmed, M.M.A., Obada, A.-S.F.: Physica A **170**, 393 (1991)
47. Vogel, W., de Matos Filho, R.L.: Phys. Rev. A **52**, 4214 (1995)
48. Wallentowitz, S., Vogel, W.: Phys. Rev. A **58**, 679 (1998)
49. Orszag, M.: Quantum Optics. Springer, New York (2000)
50. Puri, R.R., Bullough, R.K.: J. Opt. Soc. Am. B **5**, 2021 (1988)
51. Alsing, P., Zubairy, M.S.: J. Opt. Soc. Am. B **4**, 177 (1987)

52. Klimov, A.B., Negro, J., Farias, R., Chumakov, S.M.: J. Opt. B **1**, 562 (1999)
53. Warszawski, P., Wiseman, H.M.: Phys. Rev. A **63**, 013803 (2001)
54. Klein, D.J.: J. Chem. Phys. **61**, 786 (1974)
55. Shavitt, I., Redmon, L.T.: J. Chem. Phys. **73**, 5711 (1980)
56. Hashmi, F.A., Bouchene, M.A.: Appl. Math. Inform. Sci. **1**, 305 (2007)
57. Eleuch, H.: Appl. Math. Inform. Sci. **3**, 185 (2009)
58. Meekhof, D.M., Monroe, C., King, B.E., Itano, W.M., Wineland, D.J.: Phys. Rev. Lett. **76**, 1796 (1996)
59. Monroe, C., Meekhof, D.M., King, B.E., Wineland, D.J.: Science **272**, 1131 (1996)
60. Munro, W.J., Milburn, G.J., Sanders, B.C.: Phys. Rev. A **62**, 052108 (2000)
61. Kis, Z., Vogel, W., Davidovich, L.: Phys. Rev. A **64**, 033401 (2001)
62. Solano, E., de Matos Filho, R.L., Zagury, N.: Phys. Rev. Lett. **87**, 060402 (2001)
63. Solano, E., de Matos Filho, R.L., Zagury, N.: J. Opt. B: Quantum Semiclass. Opt. **4**, 324 (2002)
64. Nguyen, B.A., Truong, M.D.: Int. J. Mod. Phys. B **16**, 519 (2002)
65. Milburn, G.J.: arXiv:quant-ph/9908037 (1999)
66. Porras, D., Cirac, J.I.: arXiv:quant-ph/0401102 (2004)
67. Barjaktarevic, J.P., Milburn, G.J., McKenzie, R.H.: Phys. Rev. A **71**, 012335 (2005)
68. Yi, H.S., Nguyen, B.A., Kim, J.: J. Phys. A: Math. Gen. **37**, 11017 (2004) 6
69. Cirac, J.I., Zoller, P.: Phys. Rev. Lett. **74**, 4091 (1995)
70. Schmidt-Kaler, F., Haffner, H., Riebe, M., Gulde, S., Lancaster, G.P.T., Deuschle, T., Becher, C., Roos, C.F., Eschner, J., Blatt, R.: Nature **422**, 408 (2003)
71. Leibfried, D., Demarco, B., Meyer, V., Lucas, D., Barret, M., Britton, J., Itano, W.M., Jelenkovi, B., Langer, C., Rosenband, T., Wineland, D.J.: Nature **422**, 412 (2003)
72. Beige, A.: Phys. Rev. A **69**, 012303 (2004)
73. Monroe, C., Meekhof, D.M., King, B.E., Hano, W.M., Wineland, D.J.: Phys. Rev. Lett. **75**, 4714 (1995)
74. Monroe, C., Leibfried, D., King, B.E., Meekhof, D.M., Itano, W.M., Wineland, D.J.: Phys. Rev. A **55**, R2489 (1997)
75. Childs, A.M., Chuang, I.L.: Phys. Rev. A **63**, 012306 (2000)
76. Wei, L.F., Lei, X.L.: J. Opt. B: Quantum Semiclass. Opt. **2**, 581 (2000)
77. de Matos Filho, R.L., Vogel, W.: Phys. Rev. Lett. **76**, 608 (1996)
78. de Matos Filho, R.L., Vogel, W.: Phys. Rev. A **58**, 1661 (1998)
79. Vogel, W., Davidovich, L.: Phys. Rev. A **64**, 033401 (1996)
80. Wineland, D.J., Monroe, C., Itano, W.M., Leibfried, D., King, B.E., Meekhof, D.M.: J. Res. Natl. Inst. Stand. Technol. **103**, 259 (1998)
81. Turchette, Q.A., Wood, C.S., King, B.E., Myatt, C.J., Leibfried, D., Itano, W.M., Monroe, C., Wineland, D.J.: Phys. Rev. Lett. **81**, 3631 (1998)
82. Schwinger, J.: In: Biedenharn, L., van Dam, H. (ed.) Quantum Theory of Angular Momentum Academic, New York (1965)
83. Bermann, P.R. (ed.): Cavity Quantum Electrodynamics Supplement 2 to Advances in Atomic, Molecular, and Optical Physics. Academic, San Diego (1994)
84. Boyd, R.W.: Nonlinear Optics. Academic Press, Boston (1992)
85. Tewari, S.P., Agarwal, G.S.: Phys. Rev. Lett. **56**, 1811 (1986)
86. Li, X.S., Gong, C.D.: Phys. Rev. A **33**, 2801 (1986)
87. Napoli, A., Messina, A.: J. Mod. Opt. **43**, 649 (1996)
88. Loundon, R.: The Quantum Theory of Light. Clarendon Press, Oxford (1983)
89. Spalter, S., Burk, M., Strossner, U., Sizmann, A., Leuchs, G.: Opt. Express **2**, 77 (1998)
90. Pegg, D.T., Barnett, S.M.: Eur. Phys. Lett. **6**, 483 (1988)
91. Barnett, S.M., Pegg, D.T.: J. Mod. Opt. **36**, 7 (1989)
92. Pegg, D.T., Barnett, S.M.: Quantum Opt. **2**, 225 (1997)
93. Special issue on "Quantum phase and phase dependent measurements" of Phys. Scripta T **48** s, 1–142 (1993)
94. Lynch, R.: Phys. Rep. **256**, 367 (1995)
95. Perinova, V., Luks, A., Perina, J.: Phase in Optics. World Scientific, Singapore (1998)
96. Yamamoto, Y., Machida, S.: Phys. Rev. A **35**, 5114 (1987)
97. Wigner, E.: Phys. Rev. **40**, 749 (1932)
98. Wigner, E.: Z. Phys. Chem. B **19**, 203 (1932)
99. Sudarshan, E.C.G.: Phys. Rev. Lett. **10**, 277 (1963)
100. Obada, A.-S.F., Khalil, E.M.: Optics Commun. **260**, 19 (2006)
101. Khalil, E.M.: Int. J. Theor. Phys. **3**, 2816 (2007)
102. Husimi, K.: Proc. Phys. Math. Soc. Jpn. **22**, 264 (1940)
103. Kano, Y.: J. Math. Phys. **6**, 1913 (1965)

104. See the review Hillery, M., O'Connell, R.F., Scully, M.O., Wigner, E.P.: Phys. Rep. **106**, 121 (1984) and references therein
105. Lee, H.-W.: Phys. Rep. **259**, 147 (1995)
106. Wünsche, A.: Acta Phys. Slovaca **48**, 385 (1998)
107. Cahill, K.E., Glauber, R.J.: Phys. Rev. **177**, 1857, 1882 (1969),
108. Moya-Cessa, N., Knight, P.L.: Phys. Rev. A **48**, 2479 (1993)
109. Leonhardt, U., Paul, H.: Prog. Quantum Electron. **19**, 89 (1995)
110. Leonhardt, U.: Measuring the Quantum State of Light. Cambridge University Press, Cambridge (1997) Special issues "Quantum state preparation and measurement": Schleich, W., Raymer, M. (ed.) J. Mod. Opt. **44**(11, 12) (1997)
111. El-Orany, F.A.A., Peřina, J.: Opt. Commun. **197**, 363 (2001)
112. Wlodarz, J.J.: Phys. Lett. A **264**, 18 (1999)
113. Richter, T.: J. Mod. Opt. **48**, 1881 (2001)
114. Wünsche, A.: J. Opt. B: Quantum Semiclass. Opt. **6**, 159 (2004)
115. Mundarain, D.F., Stephany, J.: J. Phys. A: Math. Gen. **37**, 3869 (2004)
116. Khalil, E.M.: J. Phys. A: Math. Gen. **39**, 11053 (2006)
117. Agarwal, G.S., Ariunbold, G.O., Zanthier, J.V., Walther, H.: arXiv:quant-ph/0401141 (2004)
118. Benett, C.H., Brassard, G., Crepeau, C., Jozsa, R., Peres, A., Wootters, W.K.: Phys. Rev. Lett. **70**, 1895 (1993)
119. Boschi, D., Branca, S., De Martini, F., Hardy, L., Popescu, S.: Phys. Rev. Lett. **80**, 1121 (1998)
120. Bouwmeester, D., Pan, J.W., Mattle, K., Eibl, M., Weinfurter, H., Zeilinger, A.: Nature **390**, 575 (1997)
121. Furusawa, A., Sørensen, J.L., Braustein, S.L., Fuchs, C.A., Kimble, H.J., Polzik, E.S.: Science **282**, 706 (1998)
122. Lee, H.W., Kim, J.: Phys. Rev. A **63**, 012305 (2001)
123. Lombardi, E., Sciarrino, F., Popescu, S., De Martini, F.: Phys. Rev. Lett. **88**, 070402 (2002)
124. Ekert, A.K.: Phys. Rev. Lett. **67**, 661 (1991)
125. Jennewein, T., Simon, C., Weihs, G., Weinfurter, H., Zeilinger, A.: Phys. Rev. Lett. **84**, 4729 (2000)
126. Naik, D.S., Peterson, C.G., White, A.G., Berglund, A.J., Kwiat, P.G.: Phys. Rev. Lett. **84**, 4733 (2000)
127. Tittel, W., Brendel, J., Zbinden, H., Gisin, N.: Phys. Rev. Lett. **84**, 4737 (2000)
128. Lee, J.W., Lee, E.K., Chung, Y.W., Lee, H.W., Kim, J.: Phys. Rev. A **68**, 012324 (2003)
129. Raussendorf, R., Briegel, H.J.: Phys. Rev. Lett. **86**, 5188 (2001)
130. Nielsen, M.A.: Preprint arXiv:quant-ph/0402005 (2004)
131. Ahmed, M.M.A., Khalil, E.M., Obada, A.-S.F.: Opt. Commun. **254**(1), 76 (2005)
132. Obada, A.-S.F., Ahmed, M.M.A., Khalil, E.M.: J. Mod. Opt. **53**, 1149 (2006)
133. Sebawe Abdalla, M., Khalil, E.M., Obada, A.S.-F.: Ann. Phys. **11**, 2554–2568 (2007)
134. Khalil, E.M., Sebawe Abdalla, M., Obada, A.S.-F.: Ann. Phys. **321**, 421–434 (2006)
135. Khalil, E.M., Sebawe Abdalla, M., Obada, A.S.-F.: Int. J. Mod. Phys. B **18**(16), 2325 (2004)
136. Obada, A.S.-F., Sebawe Abdalla, M., Khalil, E.M.: Physica A **336**, 433 (2004)
137. Obada, A.S.-F., Sebawe Abdalla, M., Khalil, E.M.: Int. J. Theor. Phys. **42**, 2735 (2003)
138. Abdel-Aty, M., Obada, A.-S.F., Abdalla, M.S.: Int. J. Quant. Inform. **1**, 359 (2003)
139. Sebawe Abdalla, M., Obada, A.-S.F., Abdel-Aty, M.: Ann. Phys. **318**, 266 (2005)
140. Sebawe Abdalla, M., Abdel-Aty, M., Obada, A.-S.F.: Int. J. Theor. Phys. **44**, 1649 (2005)
141. Akhtarshenas, S.J., Farsi, M.: Phys. Scripta **75**, 608 (2007)
142. Bhaumik, D., Bhaumik, K., Dutta-Roy, B.: J. Phys. A: Math. Gen. **9**, 1507 (1976)
143. Agrawal, G.S.: J. Opt. Soc. Am. B **5**, 1940 (1988)
144. Knight, P.L., Radamore, P.M.: Phys. Lett. A **90**, 342 (1982)
145. Yoo, H.I., Eberly, J.H.: Phys. Rep. **118**, 239 (1981)
146. Fang, M.-F., Pengzhou, Swain, S.: J. Mod. Opt. **47**, 1043 (2000)
147. Majernikova, E., Majernik, V., Shpyrko, S.: Eur. Phys. J. B **38**, 25 (2004)
148. Majernik, V., Richterek, L.: Eur. J. Phys. **18**, 79 (1997)
149. Sanchez-Ruiz, J.: Phys. Lett. A **201**, 125 (1995)
150. Sanchez-Ruiz, J.: Phys. Lett. A **244**, 189 (1998)
151. Sanchez-Ruiz, J.: Phys. Lett. A **173**, 233 (1993)
152. Buzek, V., Keitel, C.H., Knight, P.L.: Phys. Rev. A **51**, 2575 (1995)
153. Fang, M.F., Liu, X.G.A.: Phys. Lett. A **210**, 11 (1996)
154. Abdel-Aty, M., Obada, A.-S.F., Abdalla, M.S.: J. Phys. A **34**, 912 (2001)
155. Abdel-Aty, M.: Commun. Theor. Phys. **37**, 723 (2002)